

# **Role of individual subunits in Hyperpolarization-activated cyclic nucleotide-modulated (HCN) channel gating**

## **Thesis**

in partial fulfillment of the requirements for the degree of

„Doctor rerum naturalium“ (Dr. rer. nat.)

submitted to the Council of the Faculty of Medicine

at Friedrich Schiller University of Jena

by Mallikarjuna Rao Sunkara, Master of Science (Pharm.)

born on 10.05.1988 in Machilipatnam, Andhra Pradesh, India

**Die Rolle der einzelnen Untereinheiten beim Schalten des  
durch Hyperpolarisation aktivierten und durch zyklische  
Nucleotide modulierten (HCN) Kanals**

**Dissertation**

zur Erlangung des akademischen Grades

„Doctorrerumnaturalium“ (Dr. rer. nat.)

vorgelegt dem Rat der Medizinischen Fakultät

der Friedrich-Schiller-Universität Jena

von Mallikarjuna Rao Sunkara, Master of Science (Pharm.)

geboren am 10.05.1988 in Machilipatnam, Andhra Pradesh, Indien

Gutachter / Reviewers:

1. Prof. Dr. Klaus Benndorf (Institut für Physiologie II, Herz-Kreislauf-Physiologie, Universitätsklinikum Jena)
2. Prof. Dr. Thomas Baukrowitz (Physiologisches Institut, Christian-Albrechts-Universität zu Kiel)
3. PD. Dr. Roland Schönherr (Institut für Molekulare Zellbiologie, Friedrich-Schiller-Universität Jena)

Tag der öffentlichen Verteidigung / Date of public disputation:

**22.10.2019**

# Table of Contents

Table of Contents.....	I -II
List of abbreviations .....	III - V
Summary.....	VI - VIII
1. Introduction .....	1 - 7
1.1 Structure of HCN channels .....	1
1.2 Distribution of HCN channels.....	3
1.3 Functional properties of HCN channels .....	4
1.4 Modulation by cyclic nucleotides .....	5
1.5 Physiological Significance of HCN channels .....	6
<i>HCN channels in the Heart</i> .....	6
<i>HCN channels in the nervous system</i> .....	6
1.6 HCN channels as drug targets .....	7
<i>Heart rate-reducing agents</i> .....	7
<i>Treatment of pain</i> .....	7
2. Objectives .....	8
3. Materials and Methods .....	9 - 15
3.1 Molecular biology .....	9
3.2 Construction of Multimeric HCN channels .....	9
3.3 Oocyte preparation and RNA injection.....	10
3.4 Electrophysiology.....	12
<i>Patch pipettes</i> .....	12
<i>Inside-out patch</i> .....	12
3.5 Data acquisition and analysis .....	14
3.6 Solutions.....	15
4. Results .....	16 - 35
4.1 Effects of covalent subunit linking in HCN2 concatamers.....	16
<i>Steady-state parameters</i> .....	16
<i>Kinetic parameters</i> .....	21
4.2 Effects of R591E mutation on voltage-induced activation in the absence of cAMP	23
<i>Steady-state parameters</i> .....	23
<i>Kinetic parameters</i> .....	24

4.3	The contribution of each subunit to cAMP-induced voltage shift ( $\Delta V_h$ ) .....	25	
4.4	The contribution of each subunit to cAMP-induced current increase.....	29	
4.5	The contribution of the subunits to the cAMP-induced acceleration of activation kinetics .....	30	
4.6	The contribution of the subunits to cAMP-induced deceleration of deactivation kinetics .....	32	
5.	Discussion.....	36 - 44	
5.1	Side effects of subunit ligation and point mutations were minor.....	37	
	<i>The concatenation technique (ligation) does not hinder channel function .....</i>	<i>37</i>	
	<i>R591E point mutation does not affect voltage-gated activation in the absence.....</i>	<i>of cAMP .....</i>	<i>37</i>
5.2	Steady-state activation and autoinhibition in tetrameric constructs.....	38	
	<i>Half occupation of the CNBD tetramer is sufficient to stabilize the open state.....</i>	<i>38</i>	
	<i>A full relief of autoinhibition requires the full occupation of the tetramer .....</i>	<i>40</i>	
5.3	HCN Gating and activation energetics.....	41	
6.	Conclusions .....	45	
7.	References .....	46 - 56	
8.	Appendices .....	IX - XI	
	Declaration .....	IX - X	
	Acknowledgements .....	XI	

## List of abbreviations

A	Arginine
Ag/ AgCl	Silver/ Silver chloride
Ba <sup>+2</sup>	Barium ion
Ca(NO <sub>3</sub> ) <sub>2</sub>	Calcium nitrate
Ca <sup>+2</sup>	Calcium ion
CaCl <sub>2</sub>	Calcium chloride
cAMP	Adenosine 3', 5' -cyclic monophosphate
cCMP	Cytidine 3', 5' -cyclic monophosphate
cGMP	Guanosine 3', 5' -cyclic monophosphate
cIMP	Inosine 3', 5' -cyclic monophosphate
CL	C- linker
CNBD	Cyclic nucleotide binding site
CNG	Cyclic nucleotide-gated channels
cPMP	Purine 3', 5' -cyclic monophosphate
cRNA	Complementary RNA
Cs <sup>+</sup>	Cesium ion
csd	cAMP sensing domain
cUMP	Uridine 3', 5' -cyclic monophosphate
E	Glutamate
$E_a$	Activation energy
$EC_{50}$	The concentration of the cyclic nucleotide that activates 50% of maximum current
<i>EcoRI</i>	<i>Escherichia coli</i> nuclease I from strain R
EGTA	Ethylene glycol-bis(β-aminoethyl ether)- <i>N,N,N', N'</i> -tetraacetic acid
ENaC	Epithelial Na <sup>+</sup> channels
F	Phenylalanine
$F$	Faraday constant
H	Histidine
HCN	Hyperpolarization-activated cyclic nucleotide-gated cation channel
HEPES	2- (4- (2-hydroxyethyl) -1-piperazinyl) -ethanesulfonic acid

<i>I</i>	Current
<i>I<sub>h</sub></i>	Hyperpolarization-activated currents
<i>I<sub>max</sub></i>	Maximum current
$K^+$	Potassium Ion
KCl	Potassium chloride
kHz	Kilohertz
$K_v$	Voltage-gated potassium channels
L	Lysine
Mg	Magnesium
MgCl <sub>2</sub>	Magnesium chloride
MgSO <sub>4</sub>	Magnesium sulfate
min	Minute
mM	Millimolar
mm	Millimeter
ms	Millisecond
mV	Millivolt
$Na^+$	Sodium ion
NaCl	Sodium chloride
NaHCO <sub>3</sub>	Sodium bicarbonate
nl	Nanoliter
P	Proline
<i>P<sub>o</sub></i>	Open probability
pA	Picoampere
PI(4,5)P <sub>2</sub>	Phosphatidylinositol 4,5-bisphosphate
R	Arginine
<i>R</i>	Molar gas constant
S	Serine
s	Second
SA	Sino-atrial node
SEM	The standard error of the mean
<i>T</i>	Temperature in Kelvin
<i>t<sub>h</sub></i>	The time when reaching 50% of the maximum amplitude
<i>t<sub>ha</sub></i>	Time of half-maximum activation

$t_{hd}$	Time of half-maximum deactivation
TRIS	2-Amino-2-(hydroxymethyl)propane-1,3-diol
$\Delta G$	Gibbs free energy
$\Delta V_h$	The cAMP-induced shift of half-maximal activation
$\mu M$	Micromolar
$V_{command}$	Command voltage
$V_h$	The voltage of half-maximum activation, the voltage that activates 50% of the channel
Y	Tyrosine
$z\delta$	Effective gating charge, valences of the effective charge movement of the gating



## Summary

Hyperpolarization-activated cyclic nucleotide-modulated (HCN) channels are tetramers that elicit electrical rhythmicity in special brain neurons and cardiomyocytes. These channels are non-selective cationic channels which are activated by hyperpolarizing voltages and modulated by the binding of adenosine 3', 5' -cyclic monophosphate (cAMP) to the four cyclic nucleotide-binding domains (CNBD). The binding of cAMP shifts steady-state activation to more positive voltages, thereby accelerating the activation and increasing the current along with a slowing effect on deactivation.

In spite of knowing the structure of the isolated CNBDs by crystals and X-ray analysis and very recent insights into the HCN1 structure by cryo-electron microscopy, many questions on the function of these channels remain open. In particular, how the successive binding of four cyclic nucleotides is transmitted to change the operation of the channels and how the two stimuli, hyperpolarization and cAMP binding, are interlinked. So, the aim of this work was to study the role of individual subunits in the ligand (cAMP)-dependent activation and deactivation process of HCN2 channels with the help of patch-clamp technique and *Xenopus laevis* oocytes as an expression system.

This project was focused to analyze the effects of cAMP binding to the subunits of HCN2 concatameric channels with a defined number of functional CNBDs. It was found that each liganded CNBD promotes channel activation in an additive manner irrespective of their position within the tetramer. In contrast, the open probability reached its maximum already when only two subunits were liganded. However, the process of deactivation was differently influenced by cAMP binding. Liganding of four, three, or at least two CNBDs in trans position slowed the deactivation process, whereas channels with either two functional CNBDs in cis position or with a single functional subunit were ineffective to decelerate the deactivation process.

Together the results showed herein support an activation mechanism in which each single liganded CNBD (out of four) supports channel opening by causing a turning momentum on the tetrameric intracellular gating ring, thereby stabilizing the open pore. For maintaining activation, however, at least two subunits in trans position are needed to be liganded.

## [German translation]

### **Zusammenfassung**

Durch Hyperpolarisation aktivierte und zyklische Nukleotide modulierte (HCN-) Kanäle sind Tetramere, die die elektrische Rhythmizität in spezialisierten Neuronen und Herzzellen vermitteln. Sie sind nicht-selektive Kationenkanäle, die durch Hyperpolarisation geöffnet und durch die Bindung von zyklischem Adenosinmonophosphat (cAMP) an vier intrazelluläre Bindungsstellen (CNBDs) moduliert werden. Die Bindung von cAMP führt zu einer Verschiebung der Gleichgewichts-Aktivierung zu positiveren Spannungen, zu einer Beschleunigung der Aktivierung, zu einer Zunahme der Stromamplitude bei sättigender Hyperpolarisation sowie zu einer Verlangsamung der Deaktivierung.

Trotz der Aufklärung der Struktur isolierter Bindungsstellen, sowie eines gesamten HCN-Kanals durch Röntgenstrukturanalyse bzw. Cryo-Elektronenmikroskopie, bleiben viele Fragen bezüglich des Kanalverhaltens offen. Dazu gehört die Frage, wie die Bindung der zyklischen Nukleotide in eine Konformationsänderung der Pore übersetzt wird und wie die beiden Stimuli Spannung und cAMP zusammenwirken. Ziel dieser Studie war es daher, die Rolle der individuellen Untereinheiten in der ligandenabhängigen Kanalaktivierung und –deaktivierung mit Hilfe der Patch-Clamp-Technik unter Verwendung von *Xenopus laevis*-Oozyten als heterologem Expressionssystem zu untersuchen.

Dabei lag der Fokus auf der Analyse des cAMP-abhängigen Schaltens in konkatenierten HCN2-Kanälen mit einer definierten Anzahl funktioneller Bindungsstellen. Es konnte gezeigt werden, dass jede ligandierte Bindungsstelle die Kanalaktivierung fördert und in einer additiven Weise zur cAMP-abhängigen Verschiebung der halbmaximalen Spannung beiträgt. Dabei spielt die Position innerhalb des Tetramers keine Rolle. Die maximale Offenwahrscheinlichkeit dagegen wurde bereits durch die Ligandierung von nur zwei Bindungsstellen erreicht. Auch in diesem Fall war die Position der zwei besetzten Bindungsstellen im Tetramer nicht relevant. Im Fall der Deaktivierung ist dagegen die Position der Besetzung wichtig: Nur die Ligandierung von vier, drei oder zwei Bindungsstellen in trans-Position konnte die Deaktivierung verlangsamen. Die Besetzung von zwei Bindungsstellen in cis-Position bzw. von nur einer Bindungsstelle blieb wirkungslos.

Zusammenfassend unterstützen die vorliegenden Ergebnisse einen Aktivierungsmechanismus, in dem jede einzelne ligandierte Bindungsstelle die Öffnung des Kanals begünstigt, indem eine Drehbewegung im intrazellulären Gatingring bewirkt wird, die den offenen Zustand des Kanals stabilisiert. Die Beibehaltung dieses offenen Zustandes erfordert mindestens zwei ligandierte Bindungsstellen in trans-Position.

# 1. Introduction

The autonomic heartbeat and the sleep-wake cycle are controlled by the bioelectrical cellular pacemakers. Hyperpolarization-activated cyclic nucleotide-gated (HCN) channels (Gauss et al., 1998; Ludwig et al., 1998; Santoro et al., 1998) are responsible for the membrane pacemaker current (Brown et al., 1979; DiFrancesco, 1993) that underlies the spontaneous generation of bioelectrical rhythms (Au et al., 2008). HCN channels were first discovered in the sino-atrial node (SA) cells and special neurons in the late 1970s and the currents were termed hyperpolarization-activated currents ( $I_h$ ) (Brown et al., 1979). HCN channels were also found in photoreceptor cells and Hippocampus pyramidal neurons (Bader et al., 1979; Halliwell & Adams, 1982).

HCN channels are transmembrane proteins that serve as voltage-gated cationic channels (Luthi & McCormick, 1998). They represent voltage-gated ion channels with ion-selectivity and gating properties. The currents from HCN channels are mixed cationic current carried both by sodium ( $\text{Na}^+$ ) and potassium ( $\text{K}^+$ ) ions. These are activated by membrane hyperpolarizing potentials (DiFrancesco, 1986; Tibbs et al., 1998) (-55 mV, which is near to the resting potential of cells) in the repolarization phase of the action potential, thereby evoking the pacemaker current,  $I_h$ . Because of this unusual biophysical profile, the hyperpolarization-activated current was originally also designated as “funny” current (Brown et al., 1979).

## 1.1 Structure of HCN channels

HCN channels are tetramers and belong structurally to the superfamily of tetrameric voltage-gated ion channels (Yellen, 2002; Yu et al., 2005), in particular to cyclic-nucleotide-gated (CNG) and voltage-dependent  $\text{K}^+$  ( $\text{K}_v$ ) channels (Clapham, 1998). The cartoon structure of an HCN tetramer along with a view of a monomer is shown in Figure 1.

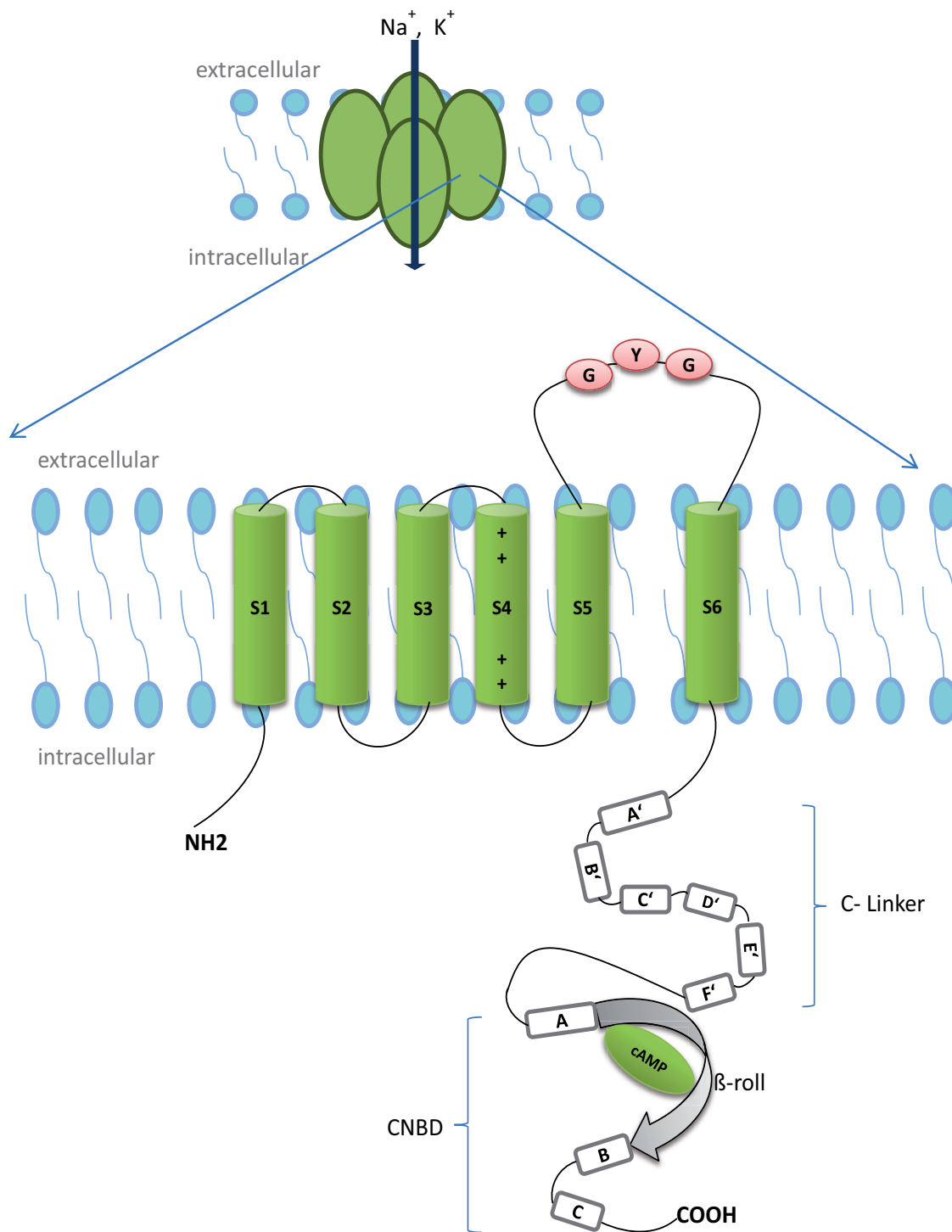


Figure 1: Structure of a HCN channel tetramer. An HCN channel subunit contains six transmembrane domains S1-S6. The S4 domain possesses a positively charged voltage sensor. The ion conducting pore with the GYG selectivity filter lies between S5 and S6. The “cAMP sensing domain” (csd) lies intracellularly between the S6 domain and the C-terminus. cAMP binds to the  $\beta$ -roll of the CNBD.

Each HCN monomer consists of six transmembrane helices (S1-S6) including the positively charged voltage sensor-S4 and the pore region contributing to the wall of a pore, between S5 and S6. This pore region contains the selectivity filter (Doyle et al., 1998) carrying the glycine-tyrosine-glycine (GYG) motif. Following the S6 transmembrane domain, there is a C-linker and the cyclic-nucleotide binding domain (CNBD), which differs from most of the other members of this superfamily (Santoro et al., 1997). Four such monomers form a tetramer.

The C-linker domain consists of six  $\alpha$ - helices, designated as A' to F' along with a short P-helix. The CNBD consists of three  $\alpha$ - helices; an initial A- helix is followed by a short B-helix and a long C- helix, and a  $\beta$ - roll between the A- and B- helices (Figure 1). Together the C-linker and CNBD can be referred to as the “cAMP sensing domain”. The structure of the isolated CNBD has been resolved by crystals and X-ray analysis for three of the four mammalian HCN isoforms (Lolicato et al., 2011; Xu et al., 2010; Zagotta et al., 2003). These structures are folded in a symmetric manner, in both the absence and presence of cAMP. Very recently, cryo-electron microscopy has been successfully used to resolve the full structure of the HCN1 isoform at 3.5 Å resolution, also in the absence and presence of cAMP (Lee & MacKinnon, 2017).

## 1.2 Distribution of HCN channels

In all mammals examined so far, four HCN isoforms were identified and were encoded by four separate genes (HCN 1-4) (Santoro et al., 2000; Santoro & Tibbs, 1999; Stieber et al., 2005) which all can form functional homotetrameric channels (Ishii et al., 2001). Members of the HCN family could also be cloned from invertebrates e.g. the spHCN channel from the testicle of the purple sea urchin *Strongylocentrotus purpuratus* (Gauss et al., 1998) or the HvCNG channel from the antennae of the owl butterfly *Heliothis virescens* (Krieger et al., 1999). HCN1 channel expression was found in the SA node, neocortex, hippocampus, dorsal root ganglion, cerebellar cortex, trigeminal ganglion, and brainstem (Moosmang et al., 1999). In contrast, HCN2 is almost ubiquitously distributed across the brain regions with a prominent presence in thalamic and brainstem nuclei as well as in the heart tissue (Ludwig et al., 1998; Santoro et al., 1998). HCN3 occurs in the olfactory bulb and with moderate to high expression in hypothalamus nuclei (Ludwig et al., 1998; Ludwig et al., 1999; Santoro et al., 2000; Santoro et al., 1998). The HCN4 subunit is predominantly expressed in the adult SA

node of all mammalian species (Biel et al., 2009), and in thalamus and testis (Seifert et al., 1999). All four isoforms are found in the spinal ganglia and in the retina (Muller et al., 2003).

All HCN isoforms are highly conserved in their CNBD region and core transmembrane region (80-90% identity) (Kaupp & Seifert, 2001) but diverge in their amino- and carboxy-terminal cytoplasmic regions (Baruscotti et al., 2005). However, the individual HCN currents differ quantitatively from each other in terms of respective activation time constants, their steady-state voltage dependence, and the extent of cAMP-dependent modulation (DiFrancesco, 1981, 1991).

### **1.3 Functional properties of HCN channels**

Out of four mammalian HCN isoforms, isolated CNBD structures of three isoforms were resolved by crystals and X-ray analysis (Goldschen-Ohm et al., 2016; Lolicato et al., 2011; Xu et al., 2010; Zagotta et al., 2003). These structures are fourfold symmetric both in the presence and absence of cAMP. Very recently, a full structure of the HCN1 isoform was resolved at 3.5 Å resolutions in the absence and presence of cAMP by using cryo-electron microscopy (Lee & MacKinnon, 2017). The structural insights of Lee and MacKinnon (2017) have proposed a scenario for the duality of voltage- and cAMP-induced activation, and, moreover, also for the unusual reversed polarity of activation compared to the other channels in this superfamily which are activated not by hyperpolarization but by depolarization. For the depolarized voltage sensor of HCN1, three components are supposed to stabilize the gate in a closed position: 1) an unusually long S4 helix touching the C-linker, 2) a special packing arrangement of the S4 to S6 helices and 3) a unique 3- $\alpha$ -helical HCN domain preceding the S1 helix. Furthermore, hyperpolarization has been supposed to drive the S4 helix in a downward direction, thereby disrupting the stabilizing effects and causing movement of the S6 helices, opening the gate. For HCN channels a similar scenario has been proposed using functional approaches (J. Chen et al., 2001; Macri et al., 2009). Concerning the activating effect of cAMP, it's binding to the CNBD would evoke a concerted rotation of the tetrameric ring-like CNBD, thereby enhancing opening of the gate by promoting the disruption of the stabilizing effects. These ideas of the cAMP effect are in line with an earlier study, suggesting a binding-induced relief of autoinhibition caused by the CNBD (Wainger et al., 2001).

HCN channels are non-selective monovalent cationic channels conducting  $K^+$  as well as  $Na^+$  ions. Their relative permeability for  $K^+$  over  $Na^+$  ions is by a ratio of  $\sim 4:1$  (Lee & MacKinnon, 2017), which is not very different from CNG1A channels where the respective permeability ratio is close to 1:1 (Derebe et al., 2011; Kaupp et al., 1989). In comparison,  $K^+$  channels have a permeability ratio of potassium over sodium by greater than 1000:1 (Neyton & Miller, 1988). This difference in selectivity comes from a different selectivity filter and surrounding amino acids that interact with the filter. Supplementarily, the native  $I_h$  current can be blocked by extracellular  $Cs^+$  ions and is relatively insensitive to  $Ba^{+2}$  ions (Ludwig et al., 1998).

## 1.4 Modulation by cyclic nucleotides

Though HCN and CNG ion channels belong to the same subgroup of cyclic nucleotide-gated cation channels, HCN channels are primarily activated by hyperpolarizing voltage and are only modulated by ligand binding. In contrast, CNG channels have an obligatory requirement of binding of either cGMP- guanosine 3', 5' -cyclic monophosphate or cAMP- adenosine 3', 5' -cyclic monophosphate to open the channel (Biel & Michalakis, 2007; Kaupp & Seifert, 2002). Ligands like cGMP, cAMP, cPMP (purine 3', 5' -cyclic monophosphate), cUMP (uridine 3', 5' -cyclic monophosphate), cCMP (cytidine 3', 5' -cyclic monophosphate), cIMP (inosine 3', 5' -cyclic monophosphate), and 2-amino-cPMP can be considered as stimulatory modulators of HCN channels. Stimulatory modulators or ligands do not open these channels in the absence of membrane hyperpolarization but rather facilitate voltage-dependent activation by shifting the voltage dependence of activation to more positive voltages and maximum increase in the current (Biel et al., 2009; DiFrancesco & Tortora, 1991; Wang et al., 2002; Wang et al., 2001). A ligand exerts its action by direct binding to the CNBD of each subunit (Craven & Zagotta, 2006; DiFrancesco, 1999; Robinson & Siegelbaum, 2003; Zagotta et al., 2003). The fundamental principle underlying the ligand-dependent modulation is "disinhibition". The CL-CNBD domain in HCN channels has an autoinhibitory effect, lowering the open probability in the absence of cAMP. Binding of cAMP increases channel activity by removing the tonic autoinhibition (Wainger et al., 2001; Wang et al., 2001). The different HCN isoforms react differently to the cyclic nucleotides presence. These differences in cyclic nucleotides sensitivity are likely due to differences in the level of CNBD channel inhibition (Wainger et al., 2001).



## 1.5 Physiological Significance of HCN channels

### *HCN channels in the Heart*

Though all isoforms of HCN have been detected in the various regions of the heart, their expression level and pattern differs among the regions. HCN subunits were detected in the SA node as well as in the Purkinje fibers and in the ventricle (Ludwig et al., 1999; Moosmang et al., 2001). HCN4 makes up ~80% of SA node  $I_h$  and had been considered to be crucial for the heartbeat generation (Shi et al., 1999; Stieber et al., 2003; Thollon et al., 2007). HCN2, that makes up ~20% of SA node  $I_h$ , could be serve as a complementary channel to HCN4 (Ludwig et al., 2003). The sinus node is the primary pacemaker of the heart and the interaction of different ion channels causes the generation of spontaneous rhythmic action potentials that control the heartbeat. Pacemaker potential is characterized by the presence of a progressive diastolic depolarization.  $I_h$  is considered to play the role of the primary initiator in this diastolic depolarization because it is activated at negative voltages (Biel et al., 2009). Different ion channels contribute to the generation of a rhythm in the sinus node of the heart. The HCN channels get activated by the membrane hyperpolarization resulting in the cationic inward current which again depolarizes the cell until voltage-gated  $Ca^{2+}$  channels open and trigger a renewed action potential (Craven & Zagotta, 2006).

HCN channels also play an important role in the regulation of heartbeat by the autonomic nervous system. During sympathetic nerve stimulation, the intracellular cAMP levels are elevated and accordingly the activity of HCN channels increases. Therefore the threshold for  $Ca^{2+}$  channels was reached earlier and this shortened the diastolic depolarization phase after action potential increases the heart rate (Alig et al., 2009; Brown et al., 1979). This is opposite to the parasympathetic/vagal stimulation where the cAMP levels get reduced and the activity of HCN channels is decreased (DiFrancesco & Tromba, 1988).

### *HCN channels in the nervous system*

In many neuronal cell types, HCN current is a major determinant of neuronal excitability. HCN channels contribute to the stabilization and determination of neuronal resting membrane potential.  $I_h$  current is involved in the modulation of excitatory postsynaptic potentials and it is the most important factor in normalizing the temporal summation in CA1 pyramidal neurons (Magee, 2000; Williams & Stuart, 2000). HCN channels are important for the control

of sleep-wake rhythm via the thalamus (Luthi & McCormick, 1998). The modulation of HCN channels by cyclic nucleotides contributing to the sensitization of sensory neuron pain stimuli (Ingram & Williams, 1996), and also play a significant role in pain perception and in painful peripheral neuropathies (Chaplan et al., 2003). Other roles of HCN channels in the central and peripheral nervous system like rhythmogenesis, resonance and oscillations properties, neurotransmitter release, control of spatial working memory, motor learning, dendritic integration, and their pathological states are widely discussed in the literature (Biel et al., 2009; Sartiani et al., 2017).

## **1.6 HCN channels as drug targets**

### ***Heart rate-reducing agents***

Lowering the heart rate is one of the most important therapeutic approaches in the treatment of cardiac diseases. The already well-known bradycardiac drugs like  $\beta$ -adrenoreceptor antagonists and  $\text{Ca}^{2+}$  channel antagonists used are often limited by their adverse reactions to the vascular system and pulmonary function. Since HCN channels are not expressed in vascular and airway smooth muscles, Ivabradine was introduced into clinical use as the first therapeutic  $I_h$  blocker. It is the only commercially available specific bradycardiac agent used in the treatment of ischemic cardiomyopathy, angina and heart failure without the side effects (Borer, 2004; Sartiani et al., 2017). Unlike Ivabradine, other HCN blockers like Zatebradine, Cilobradine, and ZD7288 were not introduced into therapy and have been reported with the side effects of visual impairment due to the nonspecific block of  $I_h$  in the nervous system and retinal regions (Biel et al., 2009; Cervetto et al., 2007).

### ***Treatment of pain***

The impressive evidence of  $I_h$  modulation may be a promising approach in the treatment of central and peripheral nervous system.  $I_h$  blockers would be beneficial in analgesic therapy because of their involvement in the pathogenesis of neuropathic pain in peripheral nerves (Papp et al., 2010; Papp et al., 2006). However, the existing  $I_h$  blockers were not highly specific for this purpose without the action on SA node as a side effect. Therefore, the development of specific blockers could pave the way to unforeseen therapeutic innovation (Sartiani et al., 2017).

## 2. Objectives

HCN channels play an important role to elicit electrical rhythmicity in specialized brain neurons and cardiomyocytes. HCN channels are tetramers and composed of four subunits that are integrally embedded in the cell membrane to create an ion-conducting pore. They are primarily activated by hyperpolarizing voltage and are modulated by ligand binding. Despite various structural insights, many questions remain open, including the question how the successive binding of four cyclic nucleotides is transmitted to change the operation of these channels and how the two stimuli, hyperpolarization and ligand (cAMP) binding, are interlinked. To study the effects of functional binding domains on channel gating, concatameric HCN2 channels containing a defined number and position of functional CNBDs were constructed by mutating (R591E) the other binding sites and linking the four subunits by the concatenation technique.

The present study had then the following objectives:

- 1) To test whether the point mutations and concatenation disturb voltage activation and cAMP effects on the channel gating under both steady-state and non-steady state conditions.
- 2) To determine the contribution of each subunit to cAMP-induced voltage shift and current increase at saturating hyperpolarization.
- 3) To determine the contribution of each subunit to the cAMP-effect on the activation kinetics.
- 4) To determine the contribution of each subunit to the cAMP-effect on the deactivation kinetics.

## 3. Materials and Methods

### 3.1 Molecular biology

RNA specific for mouse HCN2 channels (mHCN2) were used to study the contribution of each cyclic-nucleotide binding site by systematically disabling one, two, three or four binding sites. Since the amino acid position 591 of mHCN2 is important for cAMP binding, a point mutation was introduced at position 591 position by replacing arginine with glutamate (R591E). The absence of the phosphate binding site by replacing arginine by glutamate abolishes the binding of cAMP to the CNBD (Tibbs et al., 1998).

To define the stoichiometry and position of the disabled binding site (s), we worked with covalently linked subunits using linkers with amino acid sequence SPFLA (Serine-Proline-Phenylalanine-Leucine-Alanine) with a technique called concatenation. The dimeric and tetrameric constructs of mHCN2 concatamers with a different stoichiometry of functional binding sites were either a gift from S. A. Siegelbaum (Ulens & Siegelbaum, 2003) or built by Gunter Ehrlich and Tina Schwabe (Institute of Physiology II, UKJ).

### 3.2 Construction of Multimeric HCN channels

If 'w' denotes in the following a wild-type subunit and 'm' a mutated subunit the tetrameric concatamers could be written in a short way as *wwww* for a concatamer consisting of four wild-type subunits (running from the N- to the C-terminus), and so on. The tetramers *mmmm*, *mmmw*, *wmwm*, *mmww* and *wwwm*, and the dimers *wm*, *mm* were kindly provided by Prof. Siegelbaum. The constructs *mm*, *mmmm*, *mmmw*, and *mmww* were modified at position 481 of each subunit by replacing a histidine residue by a tyrosine residue according to the databank sequence NM\_008226. The other tetrameric mouse HCN2 concatamers *wwww*, *mwmw*, and *wwmm* were assembled by interlinking two HCN2 subunit dimers into a single ORF as described (Ulens and Siegelbaum, 2003). The dimer *wm* was digested using BglII restriction enzyme, the pGEM-HCN2 BglII/BglII fragment was religated yielding an R591E mutant HCN2 single subunit in pGEMHEnew. Likewise, the tetramer *mmww* was cut and the pGEM-HCN2 BglII/BglII fragment religated yielding a single wild type HCN2 subunit in pGEMHEnew. From this, the remaining dimers, *ww* and *mw*, were assembled using also a described strategy (Ulens and Siegelbaum, 2003). Initially, the unique MfeI

restriction site was introduced in front of the stop codon of the wild type and R591E mutant HCN2 in-frame with the *EcoRI* restriction site present in the vector pGEMHEnew 5' of the HCN2 start codon (Ulens and Siegelbaum, 2003). Dimers were subsequently constructed by inserting an *EcoRI*/*MfeI* fragment of w or m at the *XbaI*/*MfeI* site of pGEM-HCN2 (w or m). This resulted in a short linker sequence SPFLA between the subunits. *MfeI* and *EcoRI* have compatible cohesive ends. Ligation thus removed the *MfeI* restriction site between the co-joint subunits plus the last amino acid at the end of the C-terminus of the subunit 5' of the linkage. To obtain tetramers two dimers were joined via the same approach yielding the wwww, mwmw and wwmw concatamers. The resulting HCN2 constructs were checked by restriction digestion and subsequent gel electrophoresis as well as partial sequencing. cRNAs were transcribed from cDNAs using the mMESSEGE mMACHINE T7 Kit (Ambion, Austin, TX).

In total eight tetrameric concatamers, three dimers, and two monomers were used in this work (Table 1).

### 3.3 Oocyte preparation and RNA injection

Adult female South African claw frogs *Xenopus laevis* were anesthetized (0.3% tricaine (MS-222) (Pharmaq, Fordingbridge, UK) for the surgical removal of their oocytes. The experiments involved in animal surgery were approved by the animal ethical committee of the Friedrich Schiller University of Jena and from the Thüringer Landesamt für Verbraucherschutz (authorization dates: 2013-08-30 and 2018-09-05, respectively). The methods were performed in accordance with the approved guidelines. The defolliculation of oocytes was obtained by incubating them with 3 mg/ml collagenase (Roche, Grenzach-Wyhlen, Germany) for 105 min in Ca<sup>2+</sup>-free Barth's solution. Further, the oocytes of stages IV and V were manually isolated using forceps. Glass pipettes with 2.0 mm outer and 1.6 mm inner diameter (Hilgenberg, Malsfeld, Germany) were used to inject about 40-70 nl of channel cRNA to each oocyte. cRNA encoding mHCN2 channels of *Mus musculus* (NM\_008226) and concatamers specific for homotetrameric or concatameric channels with different stoichiometries of functional binding sites as seen in Table 1 were injected. The oocytes were incubated with Barth's medium at 18°C in an incubator. The oocyte Barth's medium was replaced every 24 hours for maintaining cell quality. The vitelline membrane of the oocyte was manually peeled immediately before the patch experiments. In addition to

these oocytes, ready-to-use oocytes purchased from Ecocyte Bioscience (Castrop-Rauxel, Germany) were used in the experiments.

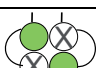
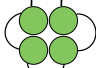
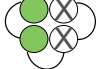
Type of constructs	Text representation	Cartoons representation
Non-concatenated subunits (Monomers)	w <sub>4</sub>	
	m <sub>4</sub>	
Dimeric concatamers	ww <sub>2</sub>	
	mm <sub>2</sub>	
	wm <sub>2</sub>	
Tetrameric concatamers	wwww	
	wwwm	
	wmwm	
	mwmw	
	mmww	
	wwmm	
	mmmw	
	mmmm	

Table 1: Constructs used in the experiments. ‘w’ denotes a wild type subunit, ‘m’ a subunit carrying the mutation R591E. The sequence of either two or four ‘w’ or ‘m’ denotes a concatamer with the respect subunit arrangement reading from N-terminus to C-terminus.

### **3.4 Electrophysiology**

The patch-clamp technique was used to study channel activation and deactivation by monitoring the ensemble current through many channels. All channels were expressed in *Xenopus laevis* oocytes. The macroscopic currents were recorded from inside-out patches of oocytes to investigate channel activation and deactivation. The patch-clamp setup was equipped with a microscope, monitor, manipulator, bath chamber, anti-vibration table, Faraday cage, head stage, amplifier, digitizer, and ISO2 hard- and software (MFK Niedernhausen, Germany). Microscope and monitor served to visualize the experiments. The manipulator allowed for 3- dimensional movements to precisely and stably positions the micropipette onto the oocyte. An anti-vibration table helped to isolate mechanical disturbances and the Faraday cage surrounding the setup eliminated electrical noise from the surrounding. A head stage that holds the micropipette transmitted the electrical signals from the micropipettes to the amplifier. A reference electrode made of Ag/AgCl (Science Products GmbH, Hofheim, Germany) was used to reduce the development of a solid-liquid junction potential between the electrode and the bath solution, and a recording electrode (Ag/AgCl wire) conducted the signal to the patch-clamp amplifier. To store the data for analysis an AD converter converted the analog signals to digital signals (12-bit resolution) using the ISO2 hard- and software. The ISO2 hard- and software was used also used to apply the voltage pulses.

#### ***Patch pipettes***

The quartz pipettes with an outer diameter of 1.0 mm, and an inner diameter of 0.7 mm (Vitrocom, New Jersey, USA) were used to measure the macroscopic currents. They were pulled from the laser puller (Model P-2000, Sutter Instrument Co., CA, USA) to get a resistance of 0.9-1.8 M $\Omega$ . Before patching, the pipettes were filled with a pipette solution filtered through 0.2  $\mu$ M non-pyrogenic filters (Sartorius stedim, Göttingen).

#### ***Inside-out patch***

Macroscopic (ensemble) currents through channels in inside-out patches obtained from the oocytes were recorded. To obtain an inside-out patch, the quartz pipette was carefully filled with pipette solution without any air bubbles. The pipette was fixed to the pipette holder and positive pressure was applied with the help of a syringe. Using a manipulator the pipette was

positioned and attached to the oocyte, and the given pressure was immediately released to obtain a Giga-seal. When the Giga-seal was stable, the pipette was quickly pulled away from the oocyte which results in the formation of the inside-out patch. After patch excision, each recording was started after 3-4 min to avoid artifacts caused by excision-induced channel rundown (Hummert et al., 2018; Thon et al., 2013). Earlier, it has been reported that the rundown caused by patch excision is at least partially caused by the dephosphorylation of PI(4,5)P<sub>2</sub>, which can be opposed by the action of a lipid kinase. This lipid kinase activity typically associated with the membrane in cell-free patches (Pian et al., 2006). In case the phosphorylation status of PI(4,5)P<sub>2</sub> is also an issue under our recording conditions, the presence of Mg<sup>2+</sup> ions should support the kinase action, thereby diminishing the rundown. For these two constructs, wmw and mmw, channel activation was tested. Their channel activation was not altered by 1 mM MgCl<sub>2</sub> (Table 2), indicating that the phosphorylation status of PI(4,5)P<sub>2</sub> was not relevant (Sunkara et al., 2018). Each excised patch was first exposed to a solution without cyclic nucleotide (bath solution) to wipe out all intrinsic cAMP molecules. Then the patch exposed to a saturating concentration of cyclic nucleotide (50 μM cAMP) to maximally activate the channel. To establish the saturation of the activating effect of 50 μM cAMP, the construct mmmw was used to compare the cAMP-induced shift of  $V_h$  ( $\Delta V_h$ ) and the percentage of cAMP-induced current increase at 50 μM with the respective data at 3 mM.  $\Delta V_h$  was  $4.8 \pm 1.1$  and  $2.4 \pm 0.5$ , and the percentage of current increase was  $7.8 \pm 0.6\%$  and  $4.2 \pm 1.2\%$ , for 50 μM and 3 mM, respectively. The respective differences were not significant (*t*-test, *P* < 0.05). Accordingly, the currents were recorded at different hyperpolarizing voltages (-70 to -150 mV), followed by a test pulse of -100 mV while holding at -30 mV (Figure 2). All experiments were performed at room temperature.

Constructs	$\Delta V_h$ without MgCl <sub>2</sub> (mV)	$\Delta V_h$ with MgCl <sub>2</sub> (mV)
wmw	$9.65 \pm 1.58$	$8.81 \pm 1.62$
mmw	$9.38 \pm 0.46$	$8.29 \pm 2.22$

Table 2: The table compares values for the cAMP-induced shift,  $\Delta V_h$  in the absence and presence of MgCl<sub>2</sub> in both control bath solution and bath solution containing 50 μM cAMP. For the tested constructs, there was no significant difference in  $\Delta V_h$  for the two constructs (*t*-test, *P* < 0.05).



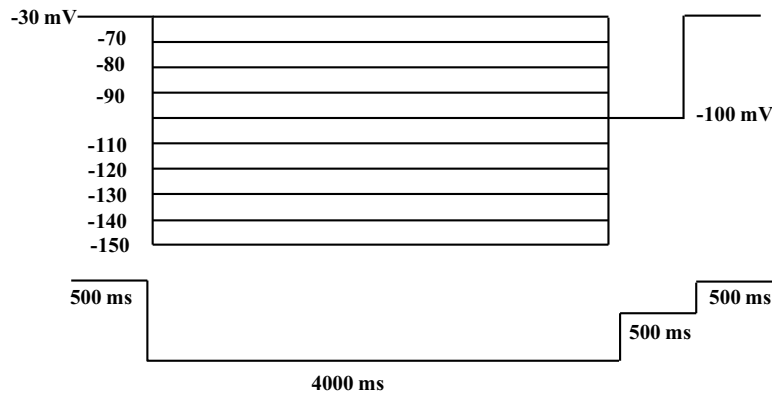


Figure 2: Schematic representation of the voltage pulse protocol along with time base. Voltages were changed with an increment of 10 mV from -70 to -150 mV.

### 3.5 Data acquisition and analysis

The amplifier Axopatch 200A (Axon Instruments) was used for current recording. As already pointed out the ISO2 hard- and software (MFK, Niedernhausen, Germany) were used to control the pulsing and data recording. The sampling rate of the recordings was 10 kHz and the recordings were on-line filtered at 2.5 kHz. Steady-state activation was determined from the amplitude of tail currents ( $I$ ) at -100 mV. All tail currents were related to the maximum tail current amplitude ( $I_{\max}$ ) as obtained at -150 mV and at saturating cAMP (50  $\mu$ M), yielding the relative current  $I/I_{\max}$  as a ratio and plotted as a function of voltage ( $V$ ) (Kusch et al., 2010)

The data points for Boltzmann relationships were fitted with OriginPro 9.0G (Northampton, USA) by the following equation:

$$I/I_{\max} = 1 / \{1 + \exp[z\delta F(V-V_h)/RT]$$

$V_h$  is the voltage of half-maximum activation, the voltage that activates 50% of the channel. The  $z\delta$  is the effective gating charge.  $F$ ,  $R$ , and  $T$  are the Faraday constant, the molar gas constant, and the temperature in Kelvin, respectively.  $I$  is the actual current amplitude and  $I_{\max}$  the maximum current amplitude at the saturating hyperpolarizing voltage of -150 mV

specified for each patch. All current amplitudes in the absence of cAMP were additionally normalized to  $I_{\max}$  at saturating cAMP.

Further, the activation and deactivation kinetics were analyzed by determining  $t_h$ , the time when reaching 50% of the maximum amplitude. Error bars indicate SEM. Fits of equations to data points were also performed with Origin 9.0G software.

### **3.6 Solutions**

The bath solution consists of (in mM) 100 KCl, 10 EGTA, 10 HEPES, and the pH was adjusted to 7.4. The pipette solution consists of (in mM) 120 KCl, 1 CaCl<sub>2</sub>, 10 HEPES and the pH was adjusted to 7.2. Ca<sup>2+</sup>-free Barth's solution containing (in mM) 82.5 NaCl, 2 KCl, 1 MgCl<sub>2</sub>, and 5 HEPES, pH 7.5 was used in the preparation of oocytes from the frog. Throughout the experiment the oocytes were maintained in Barth's medium which consists of (in mM) 84 NaCl, 1 KCl, 2.4 NaHCO<sub>3</sub>, 0.82 MgSO<sub>4</sub>, 0.41 CaCl<sub>2</sub>, 0.33 Ca(NO<sub>3</sub>)<sub>2</sub>, 7.5 TRIS, Cefuroxime, Penicillin/Streptomycin and adjusted to a pH of 7.4. The cAMP stock solution was prepared by dissolving 50 mM cAMP (Type 1, Sigma, St Louis, MO, USA) in the bath solution. The stock solutions were further diluted to achieve a final saturating concentration of 50  $\mu$ M cAMP. The concentrations of the solutions were confirmed using a UV-visible spectrophotometer. All solutions were prepared using analytical grade chemicals.

## 4. Results

### 4.1 Effects of covalent subunit linking in HCN2 concatamers

#### *Steady-state parameters*

To determine the contribution of each subunit in cyclic nucleotide cAMP binding, we constructed the tetrameric concatamers with the defined stoichiometry of functional and disabled CNBDs. For disabled CNBDs, cAMP binding was inhibited by introducing a point mutation i.e., mutating a conserved arginine (A) to glutamate (E) at position 591 (R591E) located in the beta-roll of the CNBD (Shan Chen et al., 2001; Ulens & Siegelbaum, 2003). It was previously reported that this mutation had no effect on the voltage gating in the absence of cAMP (Shan Chen et al., 2001). This mutation reduces the electrostatic interaction of cyclized phosphate of cAMP towards CNBD by more than three orders of magnitude (Shan Chen et al., 2001; Tibbs et al., 1998; Weber et al., 1987). Using concatenation, C-terminus and N-terminus of the individual subunits were ligated to make the desired stoichiometry of dimeric or tetrameric constructs. This process made the wild type concatamers of the dimer, ww, and tetramer, wwww as well as the mutated concatamers of the dimer, mm and tetramer, mmmm. In the following, a channel made from two dimers is called  $ww_2$  and  $mm_2$ , respectively. The results are discussed in the context of the channel structure.

The ionic currents from all constructs were measured with a series of hyperpolarizing pulses (from -70 to -150 mV in 10 mV increments) followed by a test pulse to -100 mV and the holding potential was -30 mV, as shown in Figure 2. The duration of hyperpolarization pulses was set to 4 s to complete channel activation at the most hyperpolarizing voltages. A typical recording of the activation for non-ligated wild type subunits,  $w_4$ , and mutated subunits,  $m_4$ , are shown in Figure 3 and Figure 4, respectively. The extent of subunit ligation disturbing the steady-state activation in wild type/mutated constructs was first tested. This was achieved by comparing the dimer and tetramer concatamers with the channels formed by the non-ligated subunits (monomers). The measuring conditions for all wild type and mutated constructs were the same. For the steady-state activation relationships, the amplitude of the instantaneous current,  $I$ , at the test pulse to -100 mV was evaluated.

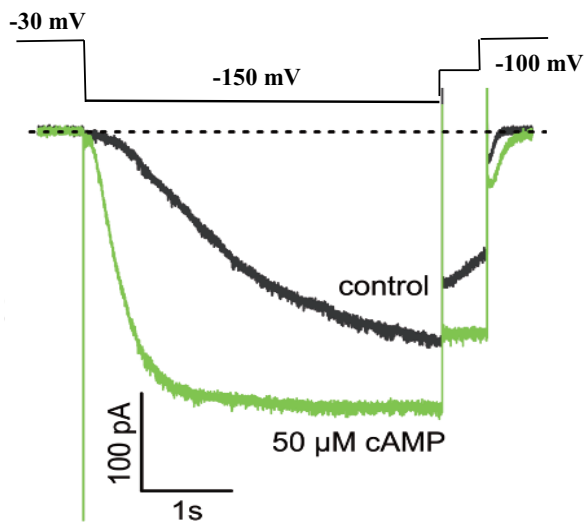


Figure 3: Representative recording for measuring steady-state activation in  $w_4$ -channels.

Typical current traces generated by the wild type construct at -150 mV in the absence and presence of 50  $\mu\text{M}$  cAMP. Black and green traces represent recordings in the absence and presence of 50  $\mu\text{M}$  cAMP, respectively.

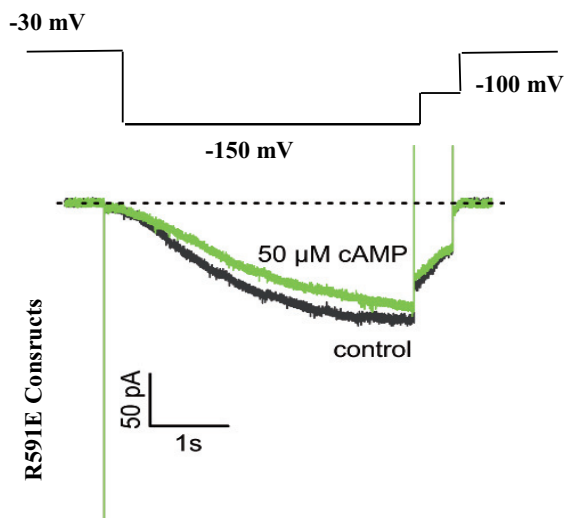


Figure 4: Representative recording for measuring steady-state activation in  $m_4$ -channels.

Typical current traces generated by the mutated construct at -150 mV in the absence and presence of 50  $\mu\text{M}$  cAMP. Black and green traces represent recordings in the absence and presence of 50  $\mu\text{M}$  cAMP, respectively.

For wild type constructs, all current amplitudes ( $I$ ) were normalized with respect to their maximum current ( $I_{\text{max}}$ ) in the presence of saturated cAMP concentration at a maximum hyperpolarizing voltage (-150 mV), which resulted for the wild type monomer,  $w_4$ , in  $I/I_{\text{max}}=0.83$  at -150 mV without cAMP. To ease further comparison,  $I/I_{\text{max}}=0.83$  was used

generally as a scaling factor for all constructs. The mean steady-state activation relationships for all wild type channels formed by the monomer ( $w_4$ ), dimer ( $ww_2$ ) and tetramer ( $wwww$ ) were plotted as  $I/I_{\max,\text{sat}}$  against voltage (mV). These wild type constructs showed the typical sigmoidal shape of the steady-state activation curve (Santoro et al., 1998) which is well established for  $w_4$  channels of HCN2 (Altomare et al., 2001). Application of cAMP at a concentration of 50  $\mu\text{M}$  allowed to open these channels completely, since their  $EC_{50}$  is  $\sim 0.1\text{-}0.3$   $\mu\text{M}$  (Ulens & Siegelbaum, 2003). At hyperpolarizing voltages, cAMP shifts the steady-state activation curve to more depolarizing potentials (less negative voltages) with an increase in current amplitude. A comparison of the steady-state activation curves for all wild type constructs  $w_4$ ,  $ww_2$ , and  $wwww$  in the absence and presence of cAMP is shown in Figure 5.

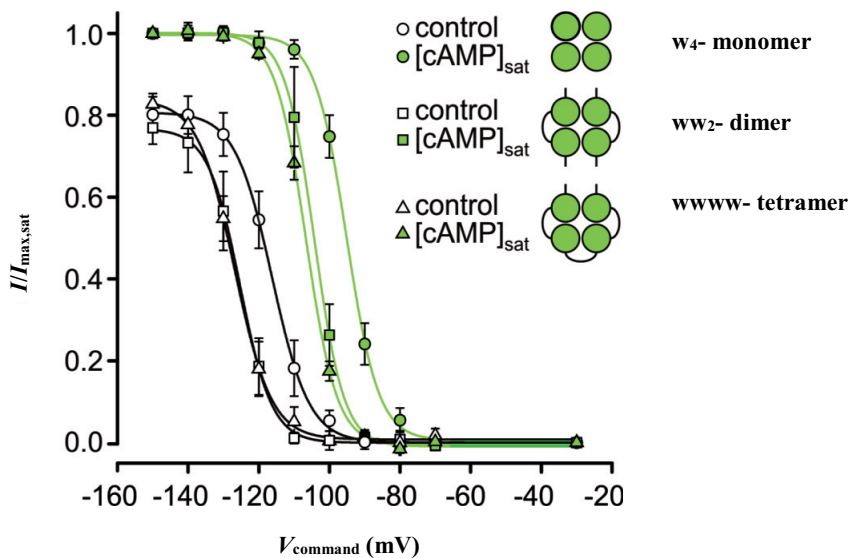


Figure 5: Steady-state activation relationships in the absence (black lines) and presence of 50  $\mu\text{M}$  cAMP (green lines) for the wild type constructs, either  $w_4$  (circles),  $ww_2$  (squares), or  $wwww$  (triangles). Assuming the maximal current for all constructs without cAMP is similar; all data were normalized with respect to the value of 0.83 of  $w_4$  at zero cAMP. Black and green curves represent activation in the absence and presence of 50  $\mu\text{M}$  cAMP, respectively. Error bars indicate SEM.

The data points of steady-state activation relationships were fitted with a Boltzmann function (Equation 1), yielding the voltage of half maximum activation,  $V_h$ , and the effective gating charge  $z\delta$ . The  $V_h$  values for the wild type constructs were  $w_4$   $-116.5 \pm 1.8$  mV,  $ww_2$   $-125.3 \pm$

2.0 mV, and *wwww*  $-123.9 \pm 2.3$  mV. In the absence of cAMP, ligation of individual subunits had a decent shift of  $V_h$  by  $\sim 10$  mV in *ww<sub>2</sub>* and *wwww* wild type constructs compared to *w<sub>4</sub>* construct, which suggests a stronger autoinhibitory effect of the CL-CNBD portion, possibly by slightly restricting the conformational movement of the N- and C-terminus. However, in the presence of cAMP, there is a cAMP-induced shift of  $V_h$  ( $\Delta V_h$ ) to a depolarized potential by an equal amount of  $\sim 20$  mV for all wild type constructs. So,  $\Delta V_h$  were not affected in *w<sub>4</sub>* (21.6 mV), *ww<sub>2</sub>* (20.9 mV), and *wwww* (21.1 mV) constructs (Figure 6, A). In addition, the  $z\delta$  values for all wild-type constructs either with or without cAMP were indistinguishable (Figure 7, A).

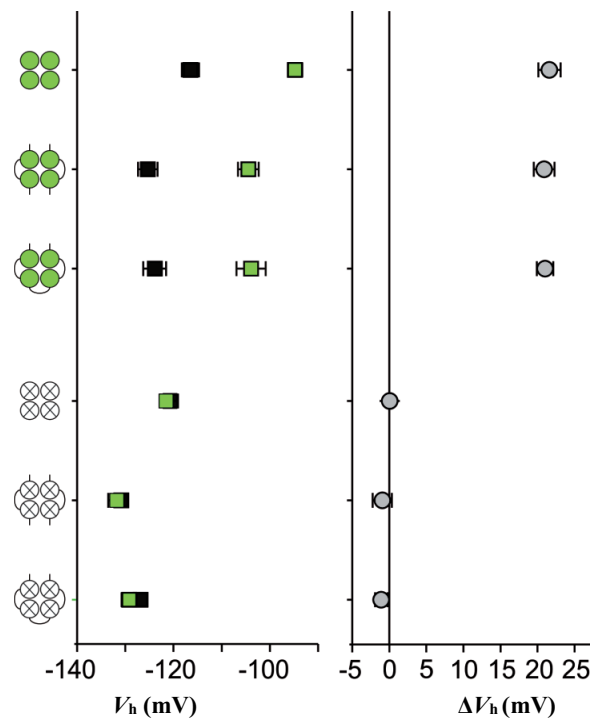


Figure 6, A: Upper part: left, the voltage of half-maximal activation ( $V_h$ ) mean values in the absence (black) and presence (green) of 50  $\mu$ M cAMP for all wild type constructs, either *w<sub>4</sub>*, *ww<sub>2</sub>* or *wwww*. Right, the cAMP-induced shift of half-maximal activation ( $\Delta V_h$ ) for all wild type constructs. Grey circles represent  $\Delta V_h$  values. Error bars indicate SEM.

Figure 6, B: Lower part: left, the voltage of half-maximal activation ( $V_h$ ) mean values in the absence (black) and presence (green) of 50  $\mu$ M cAMP for all mutated constructs, either *m<sub>4</sub>*, *mm<sub>2</sub>* or *mmmm*. Right,  $\Delta V_h$  for all mutated constructs. Grey circles represent  $\Delta V_h$  values. Error bars indicate SEM.

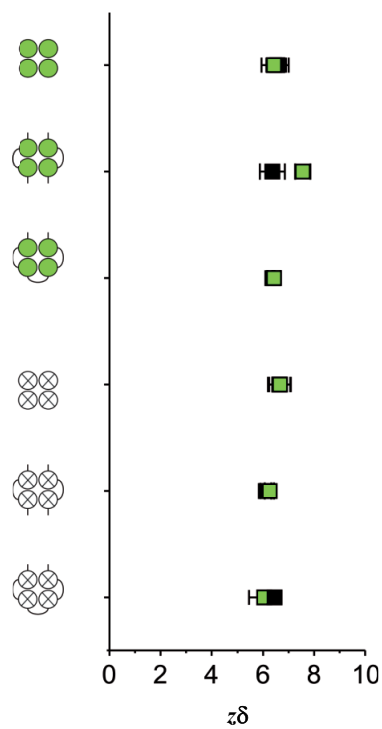


Figure 7, A: Upper part: The effective gating charge,  $z\delta$  values for all wild type constructs  $w_4$ ,  $ww_2$  or  $www$ . Error bars indicate SEM.

Figure 7, B: Lower part: The effective gating charge,  $z\delta$  values for all mutated constructs  $m_4$ ,  $mm_2$  or  $mmmm$ . Error bars indicate SEM.

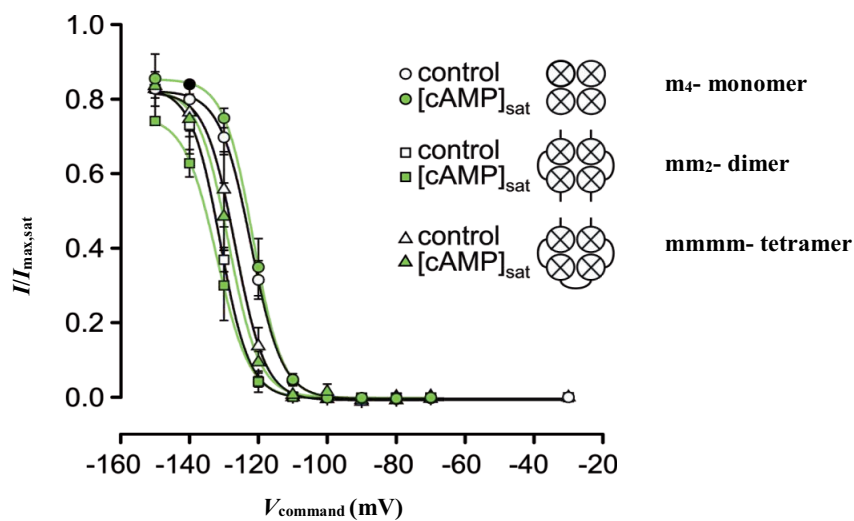


Figure 8: Steady-state activation relationships in the absence and presence of  $50 \mu\text{M}$  cAMP for all mutated constructs, either  $m_4$  (circles),  $mm_2$  (squares), or  $mmmm$  (triangles). Assuming the maximal current for all constructs without cAMP is similar; all data were normalized with respect to the value of 0.83 of  $w_4$  at zero cAMP. Black and green curves represent activation in the absence and presence of  $50 \mu\text{M}$  cAMP, respectively. Error bars indicate SEM.

For mutated constructs, the steady-state activation relationships in the absence and presence of 50  $\mu$ M cAMP were evaluated in a similar way to wild type concatamers by assuming the maximal current for all constructs without cAMP is similar.

As shown in Figure 8, all data were normalized with respect to the value of 0.83 of  $w_4$  at zero cAMP. The  $V_h$  in  $m_4$  was  $-120.7 \pm 1.6$  mV,  $mm_2$  was  $-130.9 \pm 0.6$  mV, and  $mmmm$  was  $-126.1 \pm 1.5$  mV. In comparison to wild type channels, mutated channels also had a minor effect on the voltage-dependent gating in the absence of cAMP ( $\sim$ 6-10 mV in  $mm_2$  and  $mmmm$  constructs in comparison to  $m_4$  construct). Since the binding of cAMP to these mutated constructs was limited by the point mutation, at hyperpolarizing pulses  $\Delta V_h$  was zero in Figure 6, B. Also, the effective gating charge  $z\delta$  for all the mutated constructs were indistinguishable as shown in Figure 7, B. The values of  $z\delta$  for all wild type and mutated constructs were shown in Table 3. These results summarize that covalent subunit linking does not affect their steady-state parameters, and further studies focused to study their effect on non-steady state parameters (kinetics).

### ***Kinetic parameters***

The kinetic parameter ‘time of half-maximum activation’ ( $t_{ha}$ ) was used to compare the speed of voltage-induced activation. Activation kinetics was determined for the ion channels to test their accelerating effects. The activation kinetics for all constructs were quantified by the time interval between the beginning of the clamp pulse and the half maximal current in the protocol of 4 s pulses as a time of half-maximum activation ( $t_{ha}$ ) (red lines, shown for  $wwww$  in Figure 9). We chose this simplifying measure because the true activation time course is complex (Kusch et al., 2011).

Using this method, the activation speed for the wild types  $w_4$ ,  $ww_2$ , and  $wwww$  were determined and plotted as  $t_{ha}$  vs  $V_{command}/V_h$  as shown in Figure 10. Command voltages were corrected for the differences in the steady-state activation curve by normalization with the individual  $V_h$  values. In the absence of cAMP, the voltage-dependence of the activation kinetics for wild type constructs was not changed in  $ww_2$  compared to  $w_4$ . However, linking their subunits as tetramers slowed down the activation kinetics to a very minor extent compared to the  $w_4$ . But, in the presence of 50  $\mu$ M cAMP, the given hyperpolarizing voltages made the activation kinetics faster compared to them without cAMP condition in mono, di, and tetramers (Figure 10). Similar kind of behavior was also observed with the  $m_4$ ,  $mm_2$ , and  $mmmm$  mutant constructs.



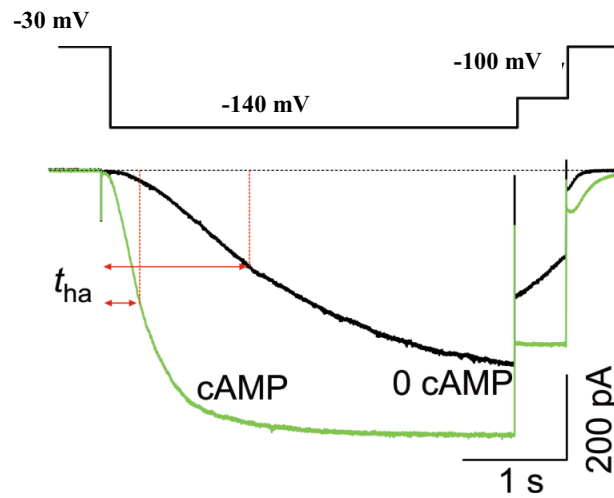


Figure 9: Representative pulse protocol and illustration of determining the time of half-maximal activation,  $t_{ha}$  (red lines). Superimposition of two activation time courses at -140 mV for wwwwww concatamer traces. Black and green curves represent in the absence and presence of 50  $\mu\text{M}$  cAMP respectively.

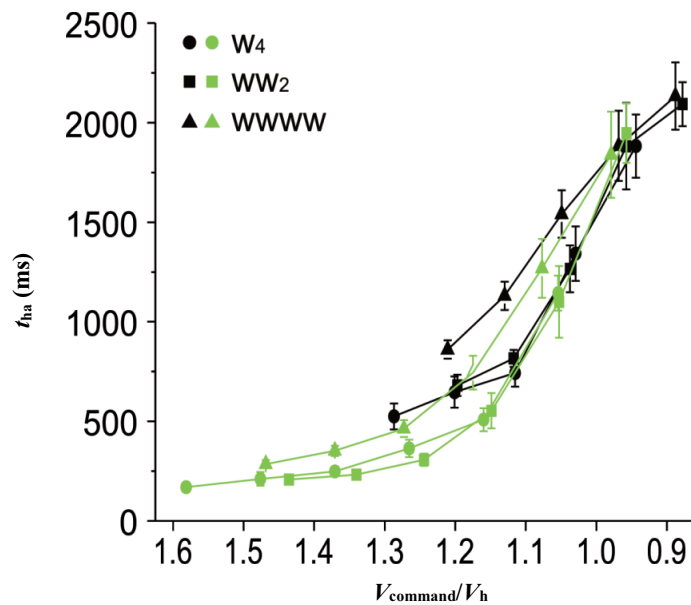


Figure 10: Time of half-maximum activation ( $t_{ha}$ ) for wild type constructs of either monomer (circles), dimer (squares), or tetramer (triangles) against normalized voltage. Black and green traces represent data in the absence and presence of 50  $\mu\text{M}$  cAMP respectively. Error bars indicate SEM.

From this, it could be concluded that linking of subunits by a short amino acid linker has a minor effect on normal channel function under both steady-state and non-steady-state conditions and for both wild type and mutated constructs. In other words, concatenation generates channels which are suitable tools for this study.

## 4.2 Effects of R591E mutation on voltage-induced activation in the absence of cAMP

### *Steady-state parameters*

In total six tetrameric concatamers with mixed subunits (wwwm, wmwm, mwmw, wwmm, mmww, mmmw) together with the two homotetramers (wwww and mmmm) were studied for their steady-state parameters. The  $V_h$  values for all constructs are plotted in Figure 11.

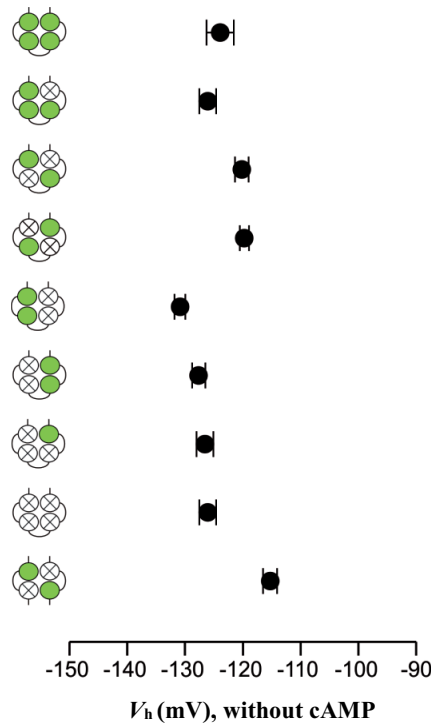


Figure 11: Effect of the R591E mutation on steady-state activation in concatamers. Comparison of half-maximum activation ( $V_h$ ) values at zero cAMP of the eight concatameric tetramers and the trans dimer  $wm_2$ . In the cartoons, green circles represent functional binding sites, whereas empty crossed circles represent mutated binding sites. Error bars indicate SEM.

At hyperpolarizing voltages and in the absence of cAMP, wwww showed a normal voltage gating with half-maximal activation,  $V_h$  of  $-123.9 \pm 2.3$  mV ( $n = 13$ ) in response to 4 s hyperpolarizing pulses duration. The  $V_h$  values for the other constructs in the absence of cAMP were: wwwm =  $-116.7 \pm 1.0$  mV ( $n = 15$ ), wmw =  $-120.2 \pm 1.2$  mV ( $n = 17$ ), mw =  $-119.7 \pm 0.8$  mV ( $n = 8$ ), mmw =  $-130.9 \pm 0.9$  mV ( $n = 14$ ), mmm =  $-126.6 \pm 0.9$  mV ( $n = 10$ ), mmm =  $-126.1 \pm 1.5$  mV ( $n = 9$ ), and trans dimer wm =  $115.3 \pm 1.2$  mV ( $n = 15$ ). Comparison of above  $V_h$  values at zero cAMP shows a similar scatter within  $\sim 10$  mV, as observed for the linking effects of wild type or mutated subunits (c.f. Figure 6).

### ***Kinetic parameters***

Constructs with linked wildtype subunits showed that linking of four subunits slowed the activation kinetics to a minor extent (c.f. Figure 10). Therefore, we tested the non-steady state activation behavior of other tetrameric concatamers. These effects were studied by the comparison of the different stoichiometric concatamers with the wildtype tetramer in the absence of cAMP as shown in Figure 12.

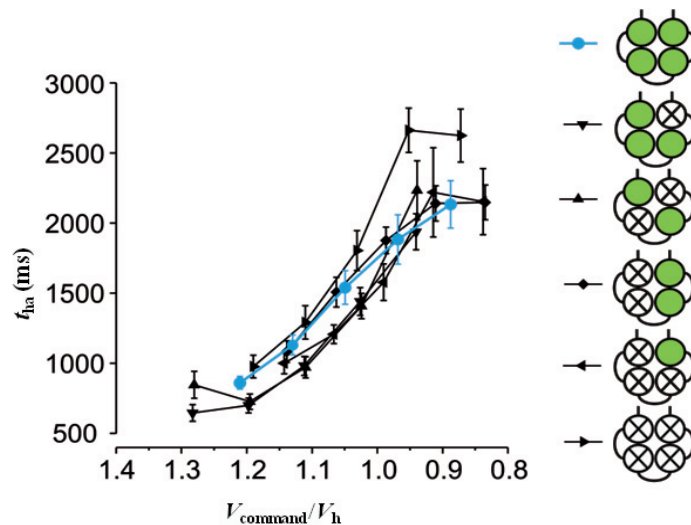


Figure 12: Time of half-maximum activation ( $t_{ha}$ ) in concatenated constructs of zero, one, two, three or four mutated binding sites against normalized voltage. Blue traces represent wild type concatenated construct. Black traces represent data in the absence of  $50 \mu\text{M}$  cAMP for concatenated constructs of one, two, three or four mutated binding sites. Error bars indicate SEM.

We observed that there was no systematic change of activation speed after introducing one, two, three and four mutated binding sites into the channel in comparison to the concatenated

wild type channel. Hence, a point mutation does not affect voltage-gated activation in the absence of cAMP. Together, these results show that side effects of point mutation and ligation of the subunits do not disturb the voltage activation and cAMP effects on the channel gating in both steady-state and non-steady state conditions. Hence, these wild type and mutated constructs do provide a useful experimental tool to study the effects of the individual subunits in detail.

### **4.3 The contribution of each subunit to cAMP-induced voltage shift ( $\Delta V_h$ )**

The binding of cAMP to the CNBD of functional subunits enhances the channel opening which resulted in both an increase of current amplitude and a shift of steady-state activation to more depolarized potentials. The steady-state activation curves for all concatamers with four, three, two, one and zero functional binding sites are shown in Figure 13. Under the experimental conditions with pulses of 4 s duration (presumably close to equilibrium), all curves were obtained by plotting  $I/I_{\max}$  values against command voltage,  $V_{\text{command}}$ , by assuming that the maximal current for all constructs without cAMP is similar. All data were normalized with respect to the value of  $I/I_{\max} = 0.83$  of  $w_4$  at zero cAMP.

All steady-state activation curves were sigmoid in shape and their slopes were indistinguishable. When cAMP was bound to the CNBD functional subunit (green traces in Figure 13), the opening of the ion channel started at less hyperpolarizing voltages compared to the cAMP-free condition (black traces in Figure 13). The ion channel opening gets increased along with the application of stronger hyperpolarizing voltages and resulted in a shift of  $V_h$  compared to the cAMP-free condition. The shift of  $V_h$  caused by bound cAMP is known as a cAMP-induced shift of  $V_h$  ( $\Delta V_h$ ) and this shift was clearly seen for all the constructs in Figure 13.

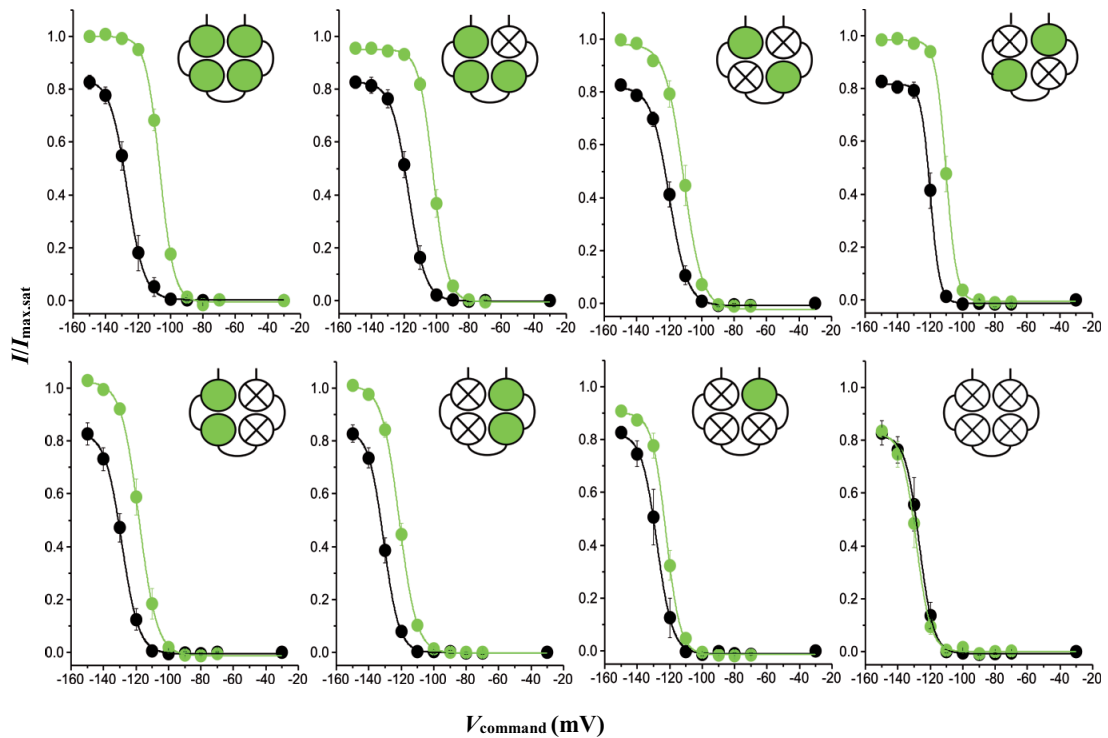


Figure 13: Steady-state activation relationships for the constructs with four, three, two, one and zero functional binding sites. Green and black traces represent conditions in the presence and absence cAMP respectively. Error bars indicate SEM.

The amount of voltage shift,  $\Delta V_h$  in all eight concatamers was in a systematic and, moreover, approximately proportional way, showing an additive effect represented in Figure 14. The additive effect is the effect of liganding a further subunit adds to the effects of other already liganded subunits. The  $\Delta V_h$  for the wild type tetramer, *wwww*, had a positive voltage shift of  $21.1 \pm 1.1$  mV similar to wild type monomer, *w*<sub>4</sub>. However, tetramers with three (*wwwm*) and one (*mmmw*) functional subunits also showed a positive voltage shift of  $14.8 \pm 1.1$  mV and  $4.8 \pm 1.1$  mV, respectively.

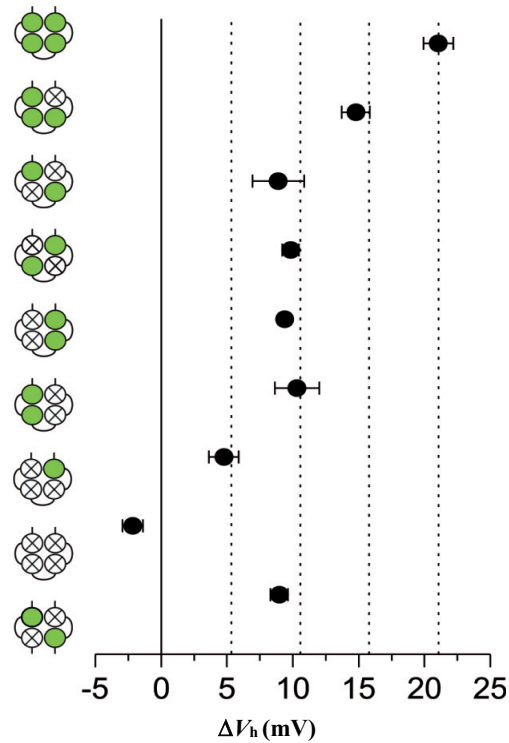


Figure 14: cAMP-induced shift of  $V_h$  ( $\Delta V_h$ ) for the constructs with four, three, two, one and zero functional binding sites. Each binding contributes to a similar extent of shift (additive effect). Cis and trans position concatamers had a similar kind of  $V_h$  shift which was further supported by the  $V_h$  shift for  $wm_2$ .

In case of tetramers with two functional subunits two cases have to be distinguished, the trans (functional binding sites were- opposite,  $wmwm$  and  $mwmw$ ) and the cis (functional binding sites were- neighbored,  $mmww$  and  $wwmm$ ) position. Both trans concatamers showed a similar positive voltage shift,  $\Delta V_h$  of  $9.7 \pm 1.6$  mV ( $wmwm$ ) and  $9.8 \pm 0.6$  mV ( $mwmw$ ). In parallel, both forms of cis also have similar positive voltage shift,  $\Delta V_h$  of  $9.4 \pm 0.5$  mV ( $mmww$ ) and  $10.3 \pm 1.7$  mV ( $wwmm$ ). Hence, in channels with two functional CNBDs, cis and trans positions exert an indistinguishable cAMP-induced voltage shift,  $\Delta V_h$ , and this was also substantially supported by the  $\Delta V_h$  of the trans dimer,  $9.0 \pm 0.7$  mV ( $wm_2$ ).

An overview of all the constructs used in the experiments along with their  $V_h$ ,  $\Delta V_h$ , and the effective gating charge  $z\delta$  values in the absence and presence of cAMP is shown in Table 3.

Constructs	$V_{h,0cAMP}$	$z\delta_{0cAMP}$	$V_{h,cAMP}$	$z\delta_{cAMP}$	$(\Delta V_h) V_{h,0cAMP}-V_{h,cAMP}$
w <sub>4</sub>	-116.5 ± 1.8	6.57 ± 0.40	-94.8 ± 1.5	6.42 ± 0.48	21.6 ± 1.1
m <sub>4</sub>	-120.7 ± 1.6	6.64 ± 0.44	-121.5 ± 1.2	6.67 ± 0.42	0.04 ± 0.7
ww <sub>2</sub>	-125.3 ± 2.0	6.36 ± 0.50	-104.5 ± 2.2	7.56 ± 0.30	20.9 ± 1.4
mm <sub>2</sub>	-130.9 ± 0.6	6.11 ± 0.21	-131.8 ± 1.7	6.26 ± 0.17	-0.94 ± 1.3
wm <sub>2</sub>	-115.3 ± 1.2	7.09 ± 0.32	-105.6 ± 1.0	6.42 ± 0.32	9.0 ± 0.7
www	-123.9 ± 2.3	6.41 ± 0.26	-103.9 ± 3.0	6.43 ± 0.26	21.1 ± 1.1
wwwm	-116.7 ± 1.0	6.00 ± 0.31	-102.0 ± 0.8	6.64 ± 0.26	14.8 ± 1.1
wmwm	-120.2 ± 1.2	6.07 ± 0.39	-111.7 ± 1.6	6.09 ± 0.34	9.7 ± 1.6
mwmw	-119.7 ± 0.8	9.03 ± 0.81	-109.9 ± 0.8	8.79 ± 0.50	9.8 ± 0.6
mmww	-130.9 ± 0.9	6.20 ± 0.20	-121.5 ± 0.9	5.25 ± 0.17	9.4 ± 0.5
wwmm	-127.6 ± 1.2	6.02 ± 0.69	-119.3 ± 1.2	5.12 ± 0.42	10.3 ± 1.7
mmmw	-126.6 ± 0.9	6.44 ± 0.46	-122.5 ± 1.1	6.30 ± 0.37	4.8 ± 1.1
mmmm	-126.1 ± 1.5	6.27 ± 0.44	-128.8 ± 1.4	6.38 ± 0.75	-2.2 ± 0.8

Table 3: Constructs used in the experiments and steady-state parameters. The data points were fitted with the Boltzmann function (equation 1), yielding the effective gating charge  $z\delta$  and the voltage of half maximum activation  $V_h$  (mV). The cAMP-induced shift of  $V_h$  ( $\Delta V_h$ , mV) was obtained from  $V_h$  values. The errors are given as SEM.

Together, an unoccupied CNBD exerts an effect on  $\Delta V_h$  irrespective of its position to the other liganded CNBDs. This suggested that a liganded CNBD causes a turning momentum on the tetrameric CNBD and that in the steep range of the concentration-activation relationship these turning momenta are additive.

#### 4.4 The contribution of each subunit to cAMP-induced current increase

The situation of cAMP-induced current increase at saturating hyperpolarizing voltage ( $\Delta I$   $-150$  mV) was notably different from the cAMP-induced voltage shift. The concatamer with four functional binding sites showed a maximum cAMP-induced current increase ( $\sim 20\%$  in Figure 15). The concatamer with one functional subunit showed only half of the effect ( $\sim 10\%$  current increase).

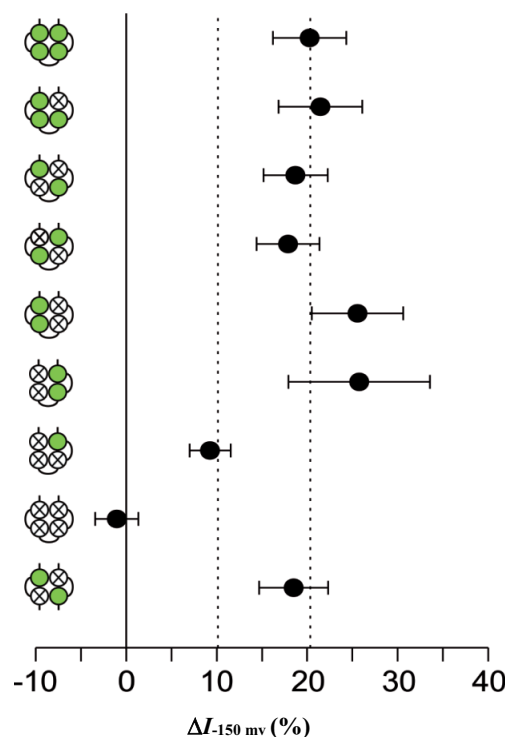


Figure 15: Effect of saturating cAMP on the current increase at the saturating voltage of  $-150$  mV,  $\Delta I$   $-150$  mV. Two liganded subunits suffice to generate the maximum effect. Data points contain 8–17 recordings. Error bars indicate SEM.

The concatamer with three functional binding sites reached also the maximal current increase similar to four functional binding sites. When two functional subunits are liganded irrespective of cis and trans positions the effect was also already maximal. This effect was further supported by the trans dimer  $wm_2$  channel (Figure 15). These data are in agreement with previous data by Zhou and Siegelbaum (2007) showing that the shift of  $V_h$  required higher cAMP concentrations



than the increase of current amplitude ( $EC_{50} = 0.1 \mu\text{M}$  vs.  $0.035 \mu\text{M}$ ) (Zhou & Siegelbaum, 2007).

These results clearly show that the cAMP-induced current increase reached a maximum with concatamers having at least two functional subunits, suggesting that the proposed turning momentum generated by at least two subunits together with the energy delivered by the strong hyperpolarization was enough to generate the maximum open probability  $P_o$ .

#### **4.5 The contribution of the subunits to the cAMP-induced acceleration of activation kinetics**

The activation kinetics was determined for all concatamers following the procedure as previously described in Figure 9. For all concatamers, the activation kinetics were plotted as the time of half-maximum activation ( $t_{ha}$ ) against hyperpolarizing voltage ( $V_{command}$ ). The activation kinetics are voltage dependent and accelerate at more negative voltages. In the absence of cAMP, all concatamers showed the typical acceleration of the activation time course at given hyperpolarizing potentials. However, in the presence of  $50 \mu\text{M}$  cAMP, HCN2 currents evoked by the voltage steps were accelerated. Further on,  $t_{ha}$  gets accelerated more depending on the number of available functional binding sites at given hyperpolarizing voltages. The activation kinetics for all constructs in the absence and presence of  $50 \mu\text{M}$  cAMP are plotted in Figure 16.

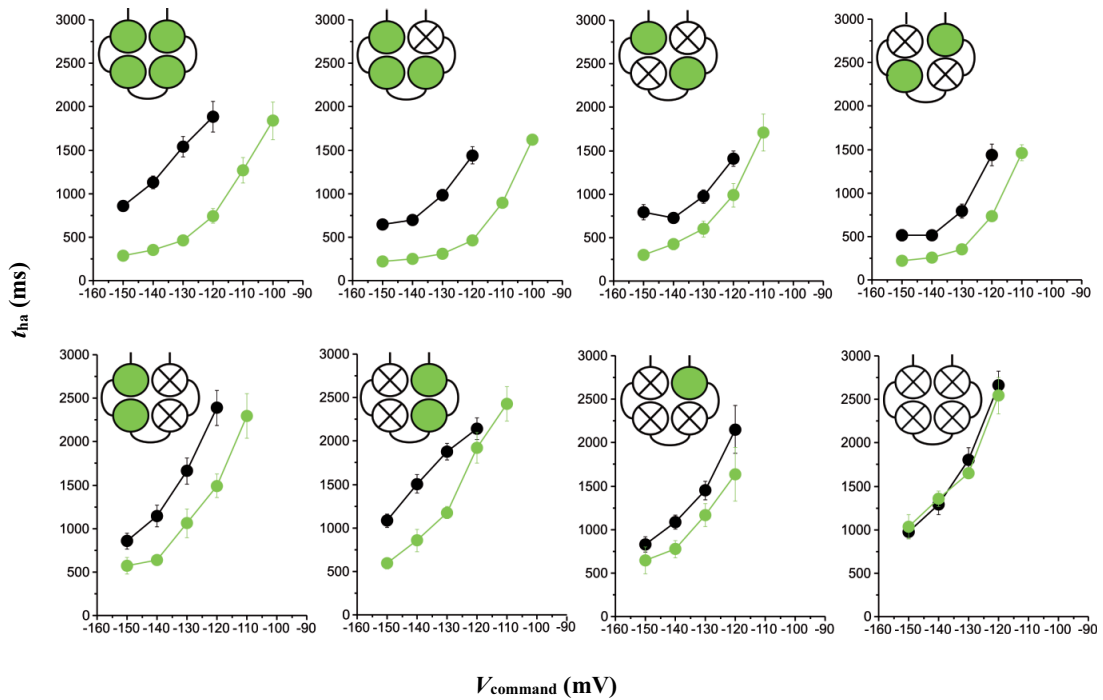


Figure 16: Time of half-maximum activation  $t_{ha}$ . The values were plotted for eight tetrameric concatamers with four, three, two, one and zero functional binding sites depending on hyperpolarizing command voltage. Error bars indicate SEM.

For comparing the accelerating effects in all constructs, data obtained at -140 mV were studied because after 4 s activation could be considered as approximately complete. For each patch, the ratio  $t_{ha,0cAMP}/t_{ha,cAMP}$  has been evaluated to minimize the variability between the activation time courses and to measure the extent of cAMP-dependent acceleration, shown in Figure 17. These ratios showed that one through four functional subunits accelerate activation in an additive manner which is a similar pattern to steady-state activation. Moreover, the four concatamers with two functional CNBDs showed no difference between cis and trans positions. This was again confirmed by the dimeric trans-channel  $wm_2$  which produced an acceleration of the activation time course similar to the respective tetramers. Apparently, the difference between three and two functional subunits was larger than the other differences. This might correspond to an earlier report showing that the third ligand binding causes the major activating effect on HCN2 channels (Kusch et al., 2011). The results of this section further support the notion that the ligand-evoked activating effects of the subunits are additive and that cis and trans concatamers produce a similar effect.

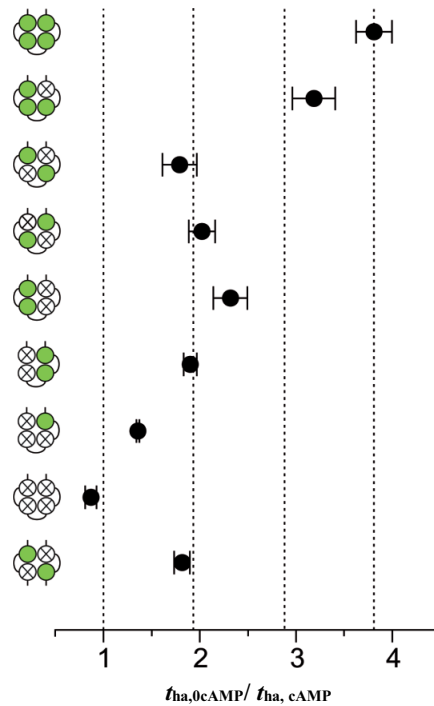


Figure 17: Comparison of time of half maximum activation ( $t_{ha}$ ) for the eight tetrameric concatamers and the trans dimeric concatamer  $wm_2$  as  $t_{ha,0cAMP} / t_{ha,cAMP}$  at hyperpolarization command voltage  $-140$  mV. Error bars indicate SEM.

#### 4.6 The contribution of the subunits to cAMP-induced deceleration of deactivation kinetics

The pathway for ligand unbinding and deactivation can be equal or different from that of ligand binding and activation. Deactivation is more closely related to the conformational changes associated with the pore action. It was quantified from deactivation time courses by evaluating the time of half maximal deactivation  $t_{hd}$ . For this, the HCN currents were activated at hyperpolarizing voltages for 6 s and  $t_{hd}$  was measured at a subsequent pulse to  $-30$  mV. The representative pulse protocol and the procedure of measuring the deactivation time courses at  $-30$  mV (inset) are shown in Figure 18.

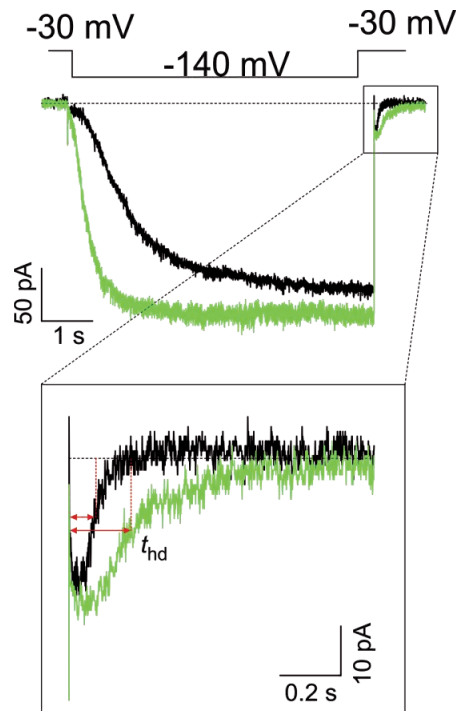


Figure 18: Determination of the time of half maximal deactivation,  $t_{hd}$  (red lines), and the pulse protocol is illustrated. The currents were activated by pulses of 6 s duration to -140 mV and deactivation was measured at a subsequent pulse to -30 mV. Superimposition of the two current time courses of the wwww concatamer in the absence and presence of cAMP and the expanded deactivation time courses at -30 mV (inset). Black and green curves indicate the absence and presence of 50  $\mu\text{M}$  cAMP, respectively.

The deactivation process proved to be independent of the hyperpolarizing voltage in the absence of ligand. Binding of cAMP, however, decelerated the deactivation kinetics, suggesting a stabilization of the open pore (Wang et al., 2002). According to Lee and MacKinnon (2017), depolarization moves the voltage sensor in an outward direction, thereby forcing the C-linker disk in a rightward rotation, keeping the gate closed. In contrast, ligand binding forces the C-linker disk into a leftward movement, the direction of gate opening (Lee & MacKinnon, 2017). These two opposing voltage-controlled forces must also form the energetic framework for the slowed deactivation at progressive liganding. To compare the deactivation kinetics in our concatamers,  $t_{hd}$  was plotted at -150, -140 and -130 mV (Figure 19).

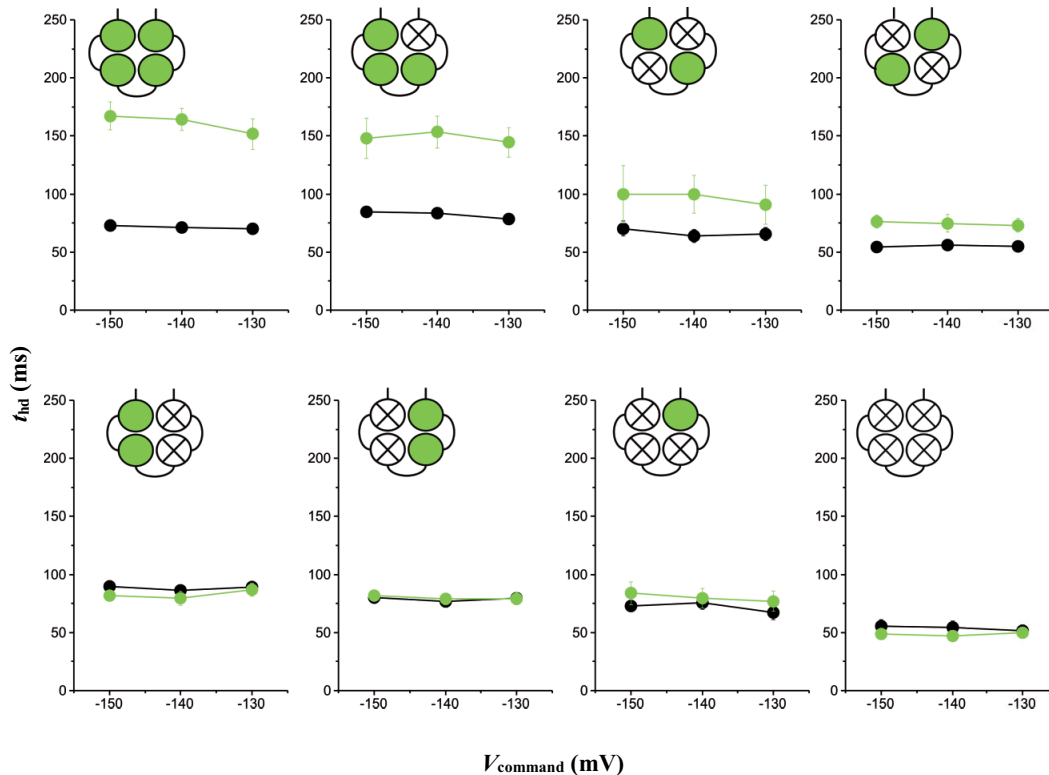


Figure 19: The time of half-maximum deactivation,  $t_{hd}$ , for eight tetrameric concatamers with four, three, two, one and zero functional binding sites in dependence on activating hyperpolarizing command voltage preceding the deactivating voltage step to -30 mV. Error bars indicate SEM.

The ligand cAMP showed a strong decelerating effect for the concatamer with four functional binding sites compared to three, two, one and zero functional binding sites. To quantify this decelerating effect, values were plotting for the time of half maximum deactivation ( $t_{hd}$ ) in the presence of 50  $\mu$ M cAMP and in the absence of cAMP as a ratio ( $t_{hd,cAMP}/t_{hd,0cAMP}$ ). The plotted ratios are shown in Figure 20. The deceleration was found to be maximal for the *wwww* concatamer with a  $t_{hd,cAMP}/t_{hd,0cAMP}$  ratio of  $\sim 2.5$ . The decelerating effect with three binding sites, *wwwm* (ratio  $\sim 2.0$ ) was less than that of *wwww*. In contrast to the additive effect of activation kinetics, the decelerating effect for two functional binding sites (*cis* and *trans*), and one functional binding site constructs were different. Concatamers with the *trans* positions (*wmwm* and *mwmw*) showed a deceleration effect with the ratio of  $\sim 1.5$ . This deceleration effect was further confirmed with the *trans* dimer, *wm<sub>2</sub>* (ratio  $\sim 1.5$ ). However, concatamers with functional CNBDs in *cis* positions, *wwmm* and *mmww*, did not show the

cAMP decelerating effect which is similar to the concatamer with one functional CNBD, mmmw. So, the concatamers with cis and trans configurations are different concerning the stabilization of the pore.

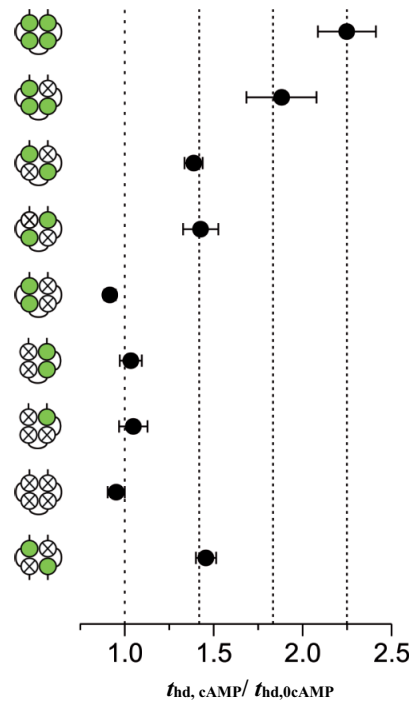


Figure 20: Comparison of  $t_{hd}$  for the eight tetrameric concatamers and the trans dimeric concatamer  $wm_2$ . Plotted is  $t_{hd,cAMP} / t_{hd,0cAMP}$  at the hyperpolarizing voltage of -140 mV. Error bars indicate SEM.

Together, these results show that subunits with four, three or at least two functional CNBDs in the trans position must be liganded to decelerate the deactivation and to stabilize the open pore. However, either of two functional CNBDs in cis position or single functional subunit is ineffective to decelerate the deactivation, i.e. to stabilize the open pore.

## 5. Discussion

This project was focused on studying the role of individual subunits in the activation gating and kinetics in HCN2 channels. It is known from earlier reports that HCN2 channel gating is dually regulated by both voltage and cyclic nucleotide binding (DiFrancesco & Tortora, 1991). The primary activating stimulus in HCN channels is membrane hyperpolarization, and channel activity is only modulated by cyclic nucleotide binding (Ludwig et al., 1998). The typical effect of cyclic nucleotide binding to HCN2 channels is to shift the half-maximum voltage to more depolarized (positive) potentials, to increase the current amplitude, and to speed up activation kinetics. The cyclic nucleotide cAMP was used as a ligand molecule in our studies to directly activate the HCN ion channels although both cAMP and cGMP are activators (DiFrancesco, 1993; Pape, 1996). HCN2 channels are much more sensitive to cAMP. Earlier studies stated that HCN2 is 60-fold more sensitive to cAMP though having a nearly identical efficacy for both cAMP and cGMP (Craven & Zagotta, 2006; Zhou & Siegelbaum, 2007).

The formation of HCN2 channel constructs having concatenated subunits with different stoichiometric of disabled CNBDs was very important in controlling of their position and cAMP binding to study the subunit positional effects. The concatenation technique was successfully implemented earlier together with a disabling of CNBDs by mutating arginine 591 to glutamate (S. Chen et al., 2001; Ulens & Siegelbaum, 2003). Therefore, liganding of specified functional subunits in HCN2 channels and voltage-dependent gating effects were successfully studied and the main results are summarized as follows: a) Binding of the ligand cAMP molecule to each subunit CNBD shifts steady-state activation to more depolarized voltages, independent on how many CNBDs are already occupied (additive effect). b) In the case of only two functional CNBDs, their trans and cis positions cause an equal voltage shift. c) The activation process becomes accelerated by subunit liganding in a respectively additive manner. d) In contrast, at saturating hyperpolarizing voltages, half occupation (two liganded subunits) causes already the maximal current increase. e) The deactivation process becomes decelerated by progressive liganding if at least two subunits in the trans position, three or four subunits are liganded whereas exclusively liganding in the cis position or only one liganded CNBD are ineffective. These summarized results are discussed in detail in the following sections.

## **5.1 Side effects of subunit ligation and point mutations were minor**

### ***The concatenation technique (ligation) does not hinder channel function***

To study the positional effects of HCN2 ion channels, tetrameric mouse HCN2 concatamers were assembled by interlinking the HCN2 subunit dimers as described in the methods part. Evidence has been provided that the concatenation technique was first successfully applied to elucidate the architecture and function of  $K^+$  channels (Isacoff et al., 1990; Liman et al., 1992). Later, it was used to study the subunit stoichiometry of other ion channels: a cyclic nucleotide-gated channel (Varnum & Zagotta, 1996; Wongsamitkul et al., 2016) the epithelial  $Na^+$  channel (Firsov et al., 1998), and P2X2 receptor (Minier & Sigel, 2004; Newbolt et al., 1998). In this study, the concatenation technique was used to link the HCN2 subunits by means of a short linker with sequence SPFLA (Ulens & Siegelbaum, 2003).

The side effects of linking were studied with control experiments to investigate if the concatamers were structurally intact and the functional properties of the channel were not influenced by this approach. For this, macroscopic currents for either wild type subunits (w-monomer, ww-dimer, www-tetramer) or mutated subunits (m-monomer, mm-dimer, mmmm-tetramer) were recorded and evaluated. It was shown that the steady-state parameters ( $V_h$ , cAMP-induced shift of  $V_h$  ( $\Delta V_h$ ), and  $z\delta$ , from Figures 5, 6, 7, 8) and kinetic parameters ( $t_{ha}$  from Figure 10) for the dimeric and tetrameric concatamers containing either wild type subunits (ww, www) or mutated subunits (mm, mmmm) fully match those of the respective channels built from their monomers. These data showed that in both wild type and mutated constructs, linking of subunits by a short amino acid linker has only negligible effects on normal channel function under steady- and non-steady state conditions. Hence, concatenated constructs are helpful tools for studies as presented herein.

### ***R591E point mutation does not affect voltage-gated activation in the absence of cAMP***

The disabling of binding sites was realized by introducing the mutation at 591 positions (R591E) in the eight stranded antiparallel  $\beta$ -roll of the CNBD. The intention of making this point mutation is to abolish the binding of cAMP to the mutated CNBDs (Tibbs et al., 1998).



However, an undesired extra mutation at position 481 was also identified in some of our constructs mm, mmmm, mmmw, and mmww. At position 481 (Y481H), in each subunit, a tyrosine residue was replaced with a histidine residue according to the data bank sequence NM\_008226. Therefore, these constructs were engineered to get free from the 481 mutation and comparison was made with the results of the cAMP-induced shift of  $V_h$ . This comparison reveals that results are identical to the results with the additional 481 mutation.

Overall, six tetrameric concatamers with mixed subunits (wwwm, wmwm, mwmw, wwmm, mmww, mmmw) together with the two homotetramers (wwww and mmmm) and a dimer  $wm_2$  were studied and evaluated. The effects of the R591E mutation for on the voltage-induced activation in the absence of cAMP were evaluated for all constructs as shown in Figure 11 by comparing the  $V_h$  values at zero cAMP. Steady-state activation of these constructs shows a similar scatter within  $\sim 10$  mV, as observed for the linking effects of wild type or mutated subunits. The effects of the R591E mutation on kinetic parameters were further supported with no systematic change in activation speed after introducing one, two, three and four mutated binding sites into the channel in comparison to the concatenated wild type channel as shown in Figure 12. Hence, a point mutation does not affect voltage-gated activation in the absence of cAMP.

Together, the above results show that side effects of the point mutation R591E and ligation of the subunits did neither disturb the voltage activation and cAMP effects on the channel gating in steady-state nor non-steady state conditions. In conclusion, these constructs provided a successful tool to monitor the role of individual subunits in HCN2 channel gating.

## **5.2 Steady-state activation and autoinhibition in tetrameric constructs**

### ***Half occupation of the CNBD tetramer is sufficient to stabilize the open state***

The effects of both cAMP and hyperpolarizing voltages on steady-state activation for all the eight concatameric tetramers and the dimer constructs were studied and summarized in Table 3. In the absence of cAMP and at strong hyperpolarization, HCN channels generate a current amplitude clearly smaller than that of fully liganded HCN channels (Seifert et al., 1999). Therefore, strong hyperpolarization alone is not sufficient to relieve the complete autoinhibition in HCN channels. Binding of cAMP to each binding site in CNBD exerts an

additional shift of steady-state activation to more depolarized voltages and an increase of current amplitude, thereby presumably relieving the autoinhibition effect and thus stabilizing an open pore.

There are two strong evidences from the results in supporting the fact that half occupation is sufficient to stabilize the open state. The first evidence is that two binding sites are sufficient to reach the maximum current increase. The binding of cAMP to the CNBD at strong hyperpolarizing voltages also generates an increase in current amplitude compared to hyperpolarizing the membrane only. This increase in current amplitude was calculated at -150 mV and plotted as  $\Delta I_{-150}$  in Figure 15. Having two functional CNBDs occupied was sufficient to generate the maximum current increase as obtained with the four occupied CNBDs, whereas occupation of a single or no binding site did not produce this effect. This effect was similar for the two occupied CNBD subunits, irrespective of cis or trans configurations and further confirmed by the trans dimer. This infers that a minimum of two functional binding sites are sufficient to produce the maximal current increase. This finding is substantiated by the previous reports in our laboratory using single-channel and patch-clamp fluorometry studies. Single-channel analysis reveals that in the presence of cAMP, the open probability ( $P_o$ ) is close to unity (Thon et al., 2013). Patch-clamp fluorometry studies provided evidence that at strong hyperpolarization, two occupied binding sites are sufficient to cause the maximum  $P_o$  (Kusch et al., 2010; Kusch et al., 2011). This illustrates that two liganded subunits along with the strong hyperpolarization were sufficient to generate the maximum  $P_o$ . Because energy is provided by the third and fourth ligand, it should be discussed that this energy can be replaced by strong hyperpolarizing voltage. In this line cAMP evoked activation with at least two ligands is needed to reach the maximum  $P_o$ . Conversely, cAMP evoked activation cannot replace voltage-evoked activation, because at depolarized voltages even the highest cAMP concentrations are ineffective to open the channels (Sunkara et al., 2018).

The second evidence is that two binding sites are sufficient to slow down the deactivation kinetics upon depolarizing voltages. In the process of deactivation, the information is quantified using deactivation kinetics and it is related to the conformational changes of pore action and its stability. Binding of cAMP to the CNBD slows down the deactivation process and this slowing effect was significantly notified with four, three and two binding sites at trans position subunits (Figures 19 and 20). However, two binding sites with cis position and

only one binding site were unable to slow down the deactivation kinetics. Though a clear additive effect was not observed in deactivation unlike in activation kinetics and steady-state voltage shift, a minimum of two binding sites in trans position is sufficient to slow down the deactivation kinetics. This confirms that trajectories for activation and deactivation are different and evidence was supported from the earlier studies of Purkinje fibers from calf hearts (DiFrancesco, 1984) or heterologously expressed HCN2 channels (Chen et al., 2007).

### ***A full relief of autoinhibition requires the full occupation of the tetramer***

In addition to current increase, cAMP binding exerts an additional shift of steady-state activation to more depolarized voltages which helps in relieving the autoinhibition effect and increasing the opening of the channel. The cAMP-induced shift,  $\Delta V_h$  for constructs with zero functional binding sites has no shift,  $m_4$  (0 mV),  $mm_2$  (-1 mV), and  $mmmm$  constructs (-2 mV) as expected. The  $\Delta V_h$  for the construct with a single functional binding site is -5 mV.  $\Delta V_h$  for the constructs with two functional binding sites  $wmwm$  and  $mmww$  was 9-10 mV. We did not observe a difference in  $\Delta V_h$  between the trans and cis concatamer. Therefore, the present results deviate from previous results showing a difference between the trans and cis constructs difference in activation gating (Ulenz & Siegelbaum, 2003). This previous study showed a significantly larger voltage shift of  $\Delta V_h$  ( $\Delta V_{1/2}$ ) of 8-9 mV in the trans concatamer  $wmwm$  compared to an only 5 mV shift in the cis concatamer  $mmww$ , leading the authors to the conclusion that the channel operates as a system of two functional dimers (Ulenz & Siegelbaum, 2003). Therefore, the present study was extended to the other possible cis and trans concatamers, cis ( $wwmm$ ) and trans ( $mwmw$ ). The  $\Delta V_h$  for the new cis ( $wwmm$ ) and trans ( $mwmw$ ) concatamers generated also a 9-10 mV shift and these results are in support of our own results. Nevertheless, the experiments in the previous study were conducted with only 1 s hyperpolarizing pulses duration (Ulenz & Siegelbaum, 2003), while in the present studies the steady-state activation was measured from the tail currents following hyperpolarizing pulses of 4 s duration. These hyperpolarizing pulses of 4 s duration are considered to be closer to the equilibrium. However, 1 s durations were also tested for some of the tetrameric constructs and the  $\Delta V_h$  values found for  $wwww$  (20 mV),  $mmmw$  (5 mV), and  $mmmm$  (1 mV) were not different from those at 4 s duration. This ascertains that the time cannot be the cause of the differences to the previous study. Therefore, this study concludes that the  $\Delta V_h$  values for all constructs with two functional binding sites have a similar cAMP-induced shift,  $\Delta V_h$  9-10 mV, irrespective of their position.

Interestingly, this  $\Delta V_h$  shift for two functional binding sites is found to be doubled in comparison to the  $\Delta V_h$  shift for a single functional binding site. This additive effect was further found in constructs with three functional binding sites, *wwwm* (15 mV) and four functional binding sites *w<sub>4</sub>*, *ww<sub>2</sub>*, and *www* (21 mV) as well. These results clearly depicted a stepwise manner of cAMP-induced shift of steady-state activation depending on the number of functional binding sites available in relieving the autoinhibition. The corresponding figures for steady-state activation were reported in Figure 13. When the  $\Delta V_h$  for four functional binding sites considered as 100% shift and comparing it with others, the  $\Delta V_h$  for three binding sites was 75% shift, for two 50% shift, for one 25% shift, for zero 0% shift as shown in Figure 14. It was shown that a maximum shift can only be reached with full-occupation. This means that two liganded subunits i.e., the half occupation of CNBDs are able to stabilize the open state but only when there is more energy provided by hyperpolarization. However, a full relief of autoinhibition requires the full occupation of the tetramer.

This additive effect was similarly observed in the activation kinetics. Subunits with one to four functional binding sites showed an acceleration of the activation kinetics in an additive manner irrespective of trans and cis positions as observed in Figure 17. However, these results were not supporting the reports of a remarkable cooperative sequence of positive-negative-positive at second, third, and fourth binding steps of HCN tetrameric channel (Kusch et al., 2011). Herein exclusively a high cAMP concentration was used that saturates all functional CNBDs independent of differences in their affinity. Therefore, complex cooperativity in the ligand binding is expected to present in all used concatamers.

### **5.3 HCN Gating and activation energetics**

For a better understanding of the voltage-dependent gating, activation, deactivation, and the pore opening behavior, a modified HCN1 channel cartoon from Lee and MacKinnon is illustrated in Figure 21 (Lee & MacKinnon, 2017). The C-linker rotation, S4- S6 domains (for only two subunits) and the S6 helix bundle are shown. According to these authors, structural features of an unusually long S4 helix and packing arrangement of S4, S5, and S6 helices empowers the depolarized voltage sensor to stabilize the closed pore. The closed gate conformation is formed by a right-handed S6 helix bundle at the inner end of the pore (Lee & MacKinnon, 2017; Rothberg et al., 2002; Shin et al., 2001). Upon membrane hyperpolarization the following structural changes help in pore opening: downward

displacement of the S4 segment to disrupt the stabilizing interactions, leftward rotation of C-linker, unwrapping and relief of S6 helix bundle pressure, and the opening of the gate. However, the autoinhibition exerted by the CL-CNBD portion does not allow the opening of the pore completely. The binding of cAMP to the hyperpolarized channel induces local conformational changes that drive the channel to further displace the S6 segment and rotate the C-linker in the direction of pore opening. Therefore, cAMP binding favors complete HCN channel opening by diminishing the autoinhibition and thus minimizing the required energy provided by voltage.

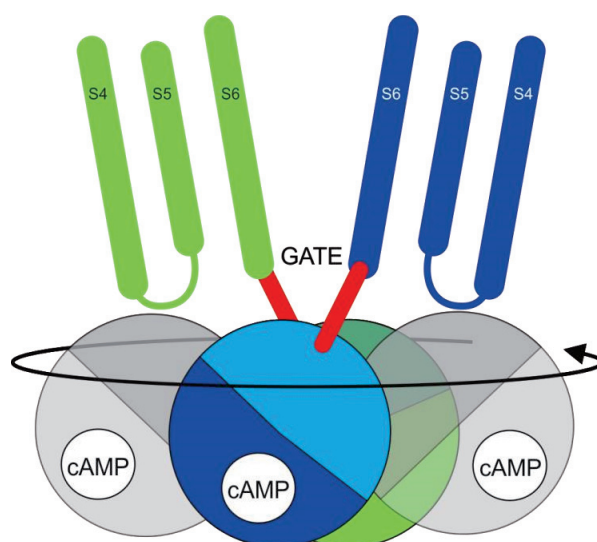


Figure 21: Gating model, a modified cartoon from (Lee & MacKinnon, 2017). Channel cartoon illustrating the C-linker rotation and S6 helix bundle (red sticks). From the transmembrane region, S4-S6 domains of only two subunits are shown here.

The idea of pore opening, turning momentum, and cAMP binding corresponds to the present results. These results showed that binding of cAMP to the constructs with one to four functional binding sites have a clear additive effect at steady-state activation and activation kinetics, irrespective of cis and trans configurations. However, cAMP must occupy all four binding sites to achieve the maximum voltage shift, acceleration of activation kinetics, and to accomplish the maximum rotation for the complete relief of autoinhibition. Non-complete occupation might cause a less pronounced rotation which brings non-complete relief of autoinhibition.

In contrast to hyperpolarization, a membrane depolarization moves the voltage sensor in an outward direction. This voltage sensor forces the C-linker in a rightward rotation in keeping the gate closed. Binding of ligand further forces the C-linker to rightward rotation of closed gate and causes slowing down of the deactivation process. This might provide a plausible explanation for slowing down of deactivation kinetics in liganded channels compared to non-liganded channels (Lee & MacKinnon, 2017). Herein, the time courses of deactivation showed that channels with two occupied CNBDs in trans position, and even more with three and four CNBDs are able to slow down the deactivation kinetics. In contrary, two occupied CNBDs in cis position, or even only one occupied CNBD, did not affect this slowing down of the process. Therefore, the trajectories for activation and deactivation in HCN channels are found to be different although deactivation is a reverse process of activation. Moreover, this concept could be explained better in terms of activation energy levels as shown in Figure 22. Though the voltage gating (Elinder et al., 2006; Mannikko et al., 2005) and cAMP binding of HCN channels (Benndorf, Kusch, et al., 2012; Benndorf, Thon, et al., 2012) are found to be complex process with multiple states involved, here in Figure 22, a channel is assumed to adopt only one open (O) and one closed (C) state.

According to the Eyring rate theory (Haring, 1942), the transition between the two states requires an amount of free energy ( $\Delta G$ ) to reach the activation energy ( $E_a$ ) of the transition state (TS). The major effect on activation is energy provided by the voltage, which is represented as thick red arrows. The energy provided by the occupancy of binding sites represented as thin red arrows. At  $-30$  mV,  $\Delta G$  is much higher in O than in C. But at  $-140$  mV,  $\Delta G$  is moderately higher in C than in O. The binding of cAMP to the four subunits (green circles) is assumed to increase and decrease  $\Delta G$  in the closed and open state, respectively. In the closed state, the energy contributions for the four binding steps are additive, whereas, in the open state, these energy contributions are only additive for the quadruple, triple, and trans-double liganded channel. This means at depolarized potentials, channels with two occupied CNBDs in trans position, and even more with three and four occupied CNBDs, require a higher activation energy  $E_a$  for inducing the process of the rightward movement of the C-linker disk. In contrast, two occupied CNBDs in cis position, or even only one occupied CNBD, do not affect this activation energy with respect to the empty channel.

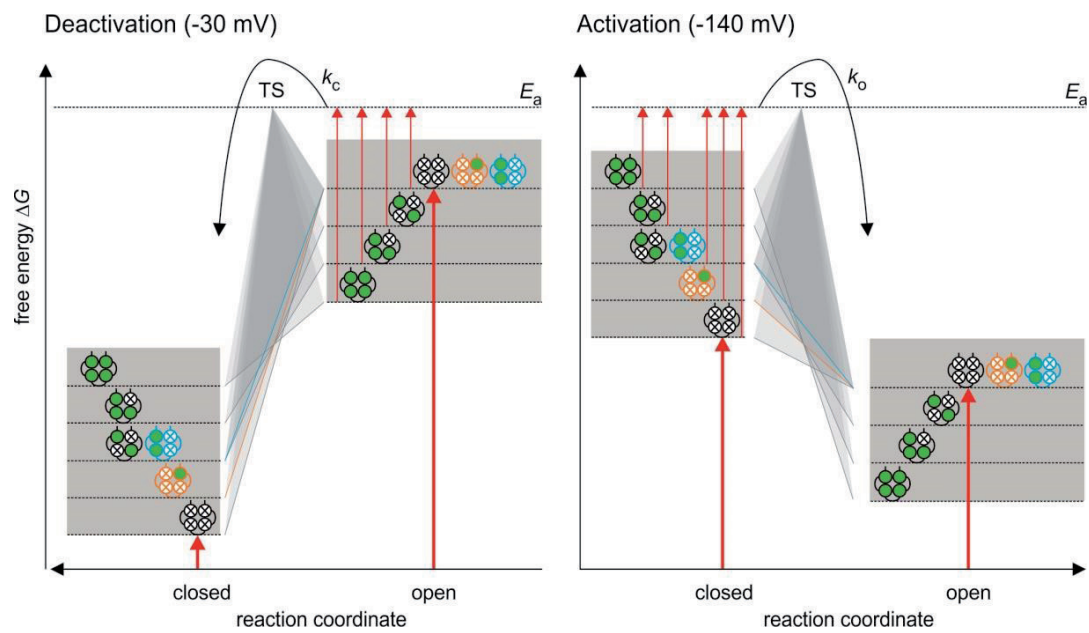


Figure 22: Cartoon model for the activation energetics by voltage and cAMP in an HCN2 channel. Energy from hyperpolarizing voltage (thick red arrows), energy from the binding of cAMP (thin red arrows), activation energy ( $E_a$ ) of the transition state (TS) for open (O) and closed (C) states. The mono-liganded and the double-liganded channel in cis position are represented with orange and blue profiles respectively.

All together these results argue for an activation mechanism in which each single liganded CNBD causes a turning momentum on the tetrameric ring-like CNBD, thereby stabilizing the open pore. But to keep this effect at least two subunits in trans position have to be liganded.

## 6. Conclusions

- 1) Linking subunits genetically does not compromise cAMP-induced HCN2 channel gating, which is shown by
  - $V_h$  shift to more depolarized voltages
  - the increase of the current amplitude
  - acceleration of activation kinetics
- 2) The R591E mutation does not compromise HCN2 activation in the absence of cAMP. Thus, concatamers with different numbers of disabled binding sites are suitable tools to study the contribution of each binding site.
- 3) Half occupation of the CNBD tetramer is sufficient to stabilize the open state, which is shown by
  - increasing the current amplitude
  - slowing down depolarization-induced deactivation
- 4) A full relief of autoinhibition requires the full occupation of the tetramer, which is shown by
  - the cAMP-induced shift of  $V_h$  ( $\Delta V_h$ )
  - speeding up hyperpolarization-induced activation
- 5) Trajectories for deactivation and activation are different, which is shown by a
  - cartoon for HCN channel gating
  - cartoon for activation energetics



## 7. References

- Alig, J., Marger, L., Mesirca, P., Ehmke, H., Mangoni, M. E., & Isbrandt, D. (2009). Control of heart rate by cAMP sensitivity of HCN channels. *Proc Natl Acad Sci U S A*, *106*(29), 12189-12194. doi:10.1073/pnas.0810332106
- Altomare, C., Bucchi, A., Camatini, E., Baruscotti, M., Viscomi, C., Moroni, A., & DiFrancesco, D. (2001). Integrated allosteric model of voltage gating of HCN channels. *J Gen Physiol*, *117*(6), 519-532.
- Au, K. W., Siu, C. W., Lau, C. P., Tse, H. F., & Li, R. A. (2008). Structural and functional determinants in the S5-P region of HCN-encoded pacemaker channels revealed by cysteine-scanning substitutions. *Am J Physiol Cell Physiol*, *294*(1), C136-144. doi:10.1152/ajpcell.00340.2007
- Bader, C. R., Macleish, P. R., & Schwartz, E. A. (1979). A voltage-clamp study of the light response in solitary rods of the tiger salamander. *J Physiol*, *296*, 1-26.
- Baruscotti, M., Bucchi, A., & DiFrancesco, D. (2005). Physiology and pharmacology of the cardiac pacemaker ("funny") current. *Pharmacol Ther*, *107*(1), 59-79. doi:10.1016/j.pharmthera.2005.01.005
- Benndorf, K., Kusch, J., & Schulz, E. (2012). Probability Fluxes and Transition Paths in a Markovian Model Describing Complex Subunit Cooperativity in HCN2 Channels. *PLoS Computational Biology*, *8*(10), e1002721. doi:10.1371/journal.pcbi.1002721
- Benndorf, K., Thon, S., & Schulz, E. (2012). Unraveling Subunit Cooperativity in Homotetrameric HCN2 Channels. *Biophysical Journal*, *103*(9), 1860-1869. doi:10.1016/j.bpj.2012.09.024
- Biel, M., & Michalakis, S. (2007). Function and dysfunction of CNG channels: insights from channelopathies and mouse models. *Mol Neurobiol*, *35*(3), 266-277.
- Biel, M., Wahl-Schott, C., Michalakis, S., & Zong, X. (2009). Hyperpolarization-activated cation channels: from genes to function. *Physiol Rev*, *89*(3), 847-885. doi:10.1152/physrev.00029.2008

- Borer, J. S. (2004). Drug insight: If inhibitors as specific heart-rate-reducing agents. *Nat Clin Pract Cardiovasc Med*, 1(2), 103-109. doi:10.1038/ncpcardio0052
- Brown, H. F., DiFrancesco, D., & Noble, S. J. (1979). How does adrenaline accelerate the heart? *Nature*, 280(5719), 235-236.
- Cervetto, L., Demontis, G. C., & Gargini, C. (2007). Cellular mechanisms underlying the pharmacological induction of phosphenes. *Br J Pharmacol*, 150(4), 383-390. doi:10.1038/sj.bjp.0706998
- Chaplan, S. R., Guo, H. Q., Lee, D. H., Luo, L., Liu, C., Kuei, C., . . . Dubin, A. E. (2003). Neuronal hyperpolarization-activated pacemaker channels drive neuropathic pain. *J Neurosci*, 23(4), 1169-1178.
- Chen, J., Mitcheson, J. S., Tristani-Firouzi, M., Lin, M., & Sanguinetti, M. C. (2001). The S4-S5 linker couples voltage sensing and activation of pacemaker channels. *Proc Natl Acad Sci U S A*, 98(20), 11277-11282. doi:10.1073/pnas.201250598
- Chen, S., Wang, J., & Siegelbaum, S. A. (2001). Properties of hyperpolarization-activated pacemaker current defined by coassembly of HCN1 and HCN2 subunits and basal modulation by cyclic nucleotide. *J Gen Physiol*, 117(5), 491-504.
- Chen, S., Wang, J., & Siegelbaum, S. A. (2001). Properties of Hyperpolarization-Activated Pacemaker Current Defined by Coassembly of Hcn1 and Hcn2 Subunits and Basal Modulation by Cyclic Nucleotide. *J Gen Physiol*, 117(5), 491-504.
- Chen, S., Wang, J., Zhou, L., George, M. S., & Siegelbaum, S. A. (2007). Voltage sensor movement and cAMP binding allosterically regulate an inherently voltage-independent closed-open transition in HCN channels. *J Gen Physiol*, 129(2), 175-188. doi:10.1085/jgp.200609585
- Clapham, D. E. (1998). Not so funny anymore: pacing channels are cloned. *Neuron*, 21(1), 5-7.
- Craven, K. B., & Zagotta, W. N. (2006). CNG and HCN channels: two peas, one pod. *Annu Rev Physiol*, 68, 375-401. doi:10.1146/annurev.physiol.68.040104.134728

- Derebe, M. G., Sauer, D. B., Zeng, W., Alam, A., Shi, N., & Jiang, Y. (2011). Tuning the ion selectivity of tetrameric cation channels by changing the number of ion binding sites. *Proc Natl Acad Sci U S A*, 108(2), 598-602. doi:10.1073/pnas.1013636108
- DiFrancesco, D. (1981). A study of the ionic nature of the pace-maker current in calf Purkinje fibres. *J Physiol*, 314, 377-393.
- DiFrancesco, D. (1984). Characterization of the pace-maker current kinetics in calf Purkinje fibres. *J Physiol*, 348, 341-367.
- DiFrancesco, D. (1986). Characterization of single pacemaker channels in cardiac sino-atrial node cells. *Nature*, 324(6096), 470-473. doi:10.1038/324470a0
- DiFrancesco, D. (1991). The contribution of the 'pacemaker' current (if) to generation of spontaneous activity in rabbit sino-atrial node myocytes. *J Physiol*, 434, 23-40.
- DiFrancesco, D. (1993). Pacemaker mechanisms in cardiac tissue. *Annu Rev Physiol*, 55, 455-472. doi:10.1146/annurev.ph.55.030193.002323
- DiFrancesco, D. (1999). Dual allosteric modulation of pacemaker (f) channels by cAMP and voltage in rabbit SA node. *J Physiol*, 515 (Pt 2), 367-376.
- DiFrancesco, D., & Tortora, P. (1991). Direct activation of cardiac pacemaker channels by intracellular cyclic AMP. *Nature*, 351(6322), 145-147. doi:10.1038/351145a0
- DiFrancesco, D., & Tromba, C. (1988). Inhibition of the hyperpolarization-activated current (if) induced by acetylcholine in rabbit sino-atrial node myocytes. *J Physiol*, 405, 477-491.
- Doyle, D. A., Morais Cabral, J., Pfuetzner, R. A., Kuo, A., Gulbis, J. M., Cohen, S. L., . . . MacKinnon, R. (1998). The structure of the potassium channel: molecular basis of K<sup>+</sup> conduction and selectivity. *Science*, 280(5360), 69-77.
- Elinder, F., Männikkö, R., Pandey, S., & Larsson, H. P. (2006). Mode shifts in the voltage gating of the mouse and human HCN2 and HCN4 channels. *J Physiol*, 575(Pt 2), 417-431. doi:10.1113/jphysiol.2006.110437

- Firsov, D., Gautschi, I., Merillat, A. M., Rossier, B. C., & Schild, L. (1998). The heterotetrameric architecture of the epithelial sodium channel (ENaC). *Embo j*, *17*(2), 344-352. doi:10.1093/emboj/17.2.344
- Gauss, R., Seifert, R., & Kaupp, U. B. (1998). Molecular identification of a hyperpolarization-activated channel in sea urchin sperm. *Nature*, *393*(6685), 583-587. doi:10.1038/31248
- Goldschen-Ohm, M. P., Klenchin, V. A., White, D. S., Cowgill, J. B., Cui, Q., Goldsmith, R. H., & Chanda, B. (2016). Structure and dynamics underlying elementary ligand binding events in human pacemaking channels. *Elife*, *5*. doi:10.7554/eLife.20797
- Halliwel, J. V., & Adams, P. R. (1982). Voltage-clamp analysis of muscarinic excitation in hippocampal neurons. *Brain Res*, *250*(1), 71-92.
- Haring, M. M. (1942). The Theory of Rate Processes (Glasstone, Samuel; Laidler, Keith J.; Eyring, Henry). *Journal of Chemical Education*, *19*(5), 249. doi:10.1021/ed019p249.1
- Hummert, S., Thon, S., Eick, T., Schmauder, R., Schulz, E., & Benndorf, K. (2018). Activation gating in HCN2 channels. *PLoS Computational Biology*, *14*(3), e1006045-e1006045. doi:10.1371/journal.pcbi.1006045
- Ingram, S. L., & Williams, J. T. (1996). Modulation of the hyperpolarization-activated current (I<sub>h</sub>) by cyclic nucleotides in guinea-pig primary afferent neurons. *J Physiol*, *492* (Pt 1), 97-106.
- Isacoff, E. Y., Jan, Y. N., & Jan, L. Y. (1990). Evidence for the formation of heteromultimeric potassium channels in *Xenopus* oocytes. *Nature*, *345*(6275), 530-534. doi:10.1038/345530a0
- Ishii, T. M., Takano, M., & Ohmori, H. (2001). Determinants of activation kinetics in mammalian hyperpolarization-activated cation channels. *J Physiol*, *537*(Pt 1), 93-100. doi:10.1111/j.1469-7793.2001.0093k.x
- Kaupp, U. B., Niidome, T., Tanabe, T., Terada, S., Bonigk, W., Stuhmer, W., . . . et al. (1989). Primary structure and functional expression from complementary DNA of the

- rod photoreceptor cyclic GMP-gated channel. *Nature*, 342(6251), 762-766. doi:10.1038/342762a0
- Kaupp, U. B., & Seifert, R. (2001). Molecular diversity of pacemaker ion channels. *Annu Rev Physiol*, 63, 235-257. doi:10.1146/annurev.physiol.63.1.235
- Kaupp, U. B., & Seifert, R. (2002). Cyclic nucleotide-gated ion channels. *Physiol Rev*, 82(3), 769-824. doi:10.1152/physrev.00008.2002
- Krieger, J., Strobel, J., Vogl, A., Hanke, W., & Breer, H. (1999). Identification of a cyclic nucleotide- and voltage-activated ion channel from insect antennae. *Insect Biochem Mol Biol*, 29(3), 255-267.
- Kusch, J., Biskup, C., Thon, S., Schulz, E., Nache, V., Zimmer, T., . . . Benndorf, K. (2010). Interdependence of receptor activation and ligand binding in HCN2 pacemaker channels. *Neuron*, 67(1), 75-85. doi:10.1016/j.neuron.2010.05.022
- Kusch, J., Thon, S., Schulz, E., Biskup, C., Nache, V., Zimmer, T., . . . Benndorf, K. (2011). How subunits cooperate in cAMP-induced activation of homotetrameric HCN2 channels. *Nat Chem Biol*, 8(2), 162-169. doi:10.1038/nchembio.747
- Lee, C. H., & MacKinnon, R. (2017). Structures of the Human HCN1 Hyperpolarization-Activated Channel. *Cell*, 168(1-2), 111-120 e111. doi:10.1016/j.cell.2016.12.023
- Liman, E. R., Tytgat, J., & Hess, P. (1992). Subunit stoichiometry of a mammalian K<sup>+</sup> channel determined by construction of multimeric cDNAs. *Neuron*, 9(5), 861-871.
- Lolicato, M., Nardini, M., Gazzarrini, S., Moller, S., Bertinetti, D., Herberg, F. W., . . . Moroni, A. (2011). Tetramerization dynamics of C-terminal domain underlies isoform-specific cAMP gating in hyperpolarization-activated cyclic nucleotide-gated channels. *J Biol Chem*, 286(52), 44811-44820. doi:10.1074/jbc.M111.297606
- Ludwig, A., Budde, T., Stieber, J., Moosmang, S., Wahl, C., Holthoff, K., . . . Hofmann, F. (2003). Absence epilepsy and sinus dysrhythmia in mice lacking the pacemaker channel HCN2. *EMBO J*, 22(2), 216-224. doi:10.1093/emboj/cdg032

- Ludwig, A., Zong, X., Jeglitsch, M., Hofmann, F., & Biel, M. (1998). A family of hyperpolarization-activated mammalian cation channels. *Nature*, *393*(6685), 587-591. doi:10.1038/31255
- Ludwig, A., Zong, X., Stieber, J., Hullin, R., Hofmann, F., & Biel, M. (1999). Two pacemaker channels from human heart with profoundly different activation kinetics. *EMBO J*, *18*(9), 2323-2329. doi:10.1093/emboj/18.9.2323
- Luthi, A., & McCormick, D. A. (1998). H-current: properties of a neuronal and network pacemaker. *Neuron*, *21*(1), 9-12.
- Macri, V., Nazzari, H., McDonald, E., & Accili, E. A. (2009). Alanine scanning of the S6 segment reveals a unique and cAMP-sensitive association between the pore and voltage-dependent opening in HCN channels. *J Biol Chem*, *284*(23), 15659-15667. doi:10.1074/jbc.M809164200
- Magee, J. C. (2000). Dendritic integration of excitatory synaptic input. *Nat Rev Neurosci*, *1*(3), 181-190. doi:10.1038/35044552
- Mannikko, R., Pandey, S., Larsson, H. P., & Elinder, F. (2005). Hysteresis in the voltage dependence of HCN channels: conversion between two modes affects pacemaker properties. *J Gen Physiol*, *125*(3), 305-326. doi:10.1085/jgp.200409130
- Minier, F., & Sigel, E. (2004). Techniques: Use of concatenated subunits for the study of ligand-gated ion channels. *Trends Pharmacol Sci*, *25*(9), 499-503. doi:10.1016/j.tips.2004.07.005
- Moosmang, S., Biel, M., Hofmann, F., & Ludwig, A. (1999). Differential distribution of four hyperpolarization-activated cation channels in mouse brain. *Biol Chem*, *380*(7-8), 975-980. doi:10.1515/bc.1999.121
- Moosmang, S., Stieber, J., Zong, X., Biel, M., Hofmann, F., & Ludwig, A. (2001). Cellular expression and functional characterization of four hyperpolarization-activated pacemaker channels in cardiac and neuronal tissues. *Eur J Biochem*, *268*(6), 1646-1652.

- Muller, F., Scholten, A., Ivanova, E., Haverkamp, S., Kremmer, E., & Kaupp, U. B. (2003). HCN channels are expressed differentially in retinal bipolar cells and concentrated at synaptic terminals. *Eur J Neurosci*, *17*(10), 2084-2096.
- Newbolt, A., Stoop, R., Virginio, C., Surprenant, A., North, R. A., Buell, G., & Rassendren, F. (1998). Membrane topology of an ATP-gated ion channel (P2X receptor). *J Biol Chem*, *273*(24), 15177-15182.
- Neyton, J., & Miller, C. (1988). Potassium blocks barium permeation through a calcium-activated potassium channel. *J Gen Physiol*, *92*(5), 549-567.
- Pape, H. C. (1996). Queer current and pacemaker: the hyperpolarization-activated cation current in neurons. *Annu Rev Physiol*, *58*, 299-327. doi:10.1146/annurev.ph.58.030196.001503
- Papp, I., Hollo, K., & Antal, M. (2010). Plasticity of hyperpolarization-activated and cyclic nucleotid-gated cation channel subunit 2 expression in the spinal dorsal horn in inflammatory pain. *Eur J Neurosci*, *32*(7), 1193-1201. doi:10.1111/j.1460-9568.2010.07370.x
- Papp, I., Szucs, P., Hollo, K., Erdelyi, F., Szabo, G., & Antal, M. (2006). Hyperpolarization-activated and cyclic nucleotide-gated cation channel subunit 2 ion channels modulate synaptic transmission from nociceptive primary afferents containing substance P to secondary sensory neurons in laminae I-IIo of the rodent spinal dorsal horn. *Eur J Neurosci*, *24*(5), 1341-1352. doi:10.1111/j.1460-9568.2006.05013.x
- Pian, P., Bucchi, A., Robinson, R. B., & Siegelbaum, S. A. (2006). Regulation of gating and rundown of HCN hyperpolarization-activated channels by exogenous and endogenous PIP2. *J Gen Physiol*, *128*(5), 593-604. doi:10.1085/jgp.200609648
- Robinson, R. B., & Siegelbaum, S. A. (2003). Hyperpolarization-activated cation currents: from molecules to physiological function. *Annu Rev Physiol*, *65*, 453-480. doi:10.1146/annurev.physiol.65.092101.142734
- Rothberg, B. S., Shin, K. S., Phale, P. S., & Yellen, G. (2002). Voltage-controlled gating at the intracellular entrance to a hyperpolarization-activated cation channel. *J Gen Physiol*, *119*(1), 83-91.

- Santoro, B., Chen, S., Luthi, A., Pavlidis, P., Shumyatsky, G. P., Tibbs, G. R., & Siegelbaum, S. A. (2000). Molecular and functional heterogeneity of hyperpolarization-activated pacemaker channels in the mouse CNS. *J Neurosci*, *20*(14), 5264-5275.
- Santoro, B., Grant, S. G., Bartsch, D., & Kandel, E. R. (1997). Interactive cloning with the SH3 domain of N-src identifies a new brain specific ion channel protein, with homology to eag and cyclic nucleotide-gated channels. *Proc Natl Acad Sci U S A*, *94*(26), 14815-14820.
- Santoro, B., Liu, D. T., Yao, H., Bartsch, D., Kandel, E. R., Siegelbaum, S. A., & Tibbs, G. R. (1998). Identification of a gene encoding a hyperpolarization-activated pacemaker channel of brain. *Cell*, *93*(5), 717-729.
- Santoro, B., & Tibbs, G. R. (1999). The HCN gene family: molecular basis of the hyperpolarization-activated pacemaker channels. *Ann N Y Acad Sci*, *868*, 741-764.
- Sartiani, L., Mannaioni, G., Masi, A., Novella Romanelli, M., & Cerbai, E. (2017). The Hyperpolarization-Activated Cyclic Nucleotide-Gated Channels: from Biophysics to Pharmacology of a Unique Family of Ion Channels. *Pharmacol Rev*, *69*(4), 354-395. doi:10.1124/pr.117.014035
- Seifert, R., Scholten, A., Gauss, R., Mincheva, A., Lichter, P., & Kaupp, U. B. (1999). Molecular characterization of a slowly gating human hyperpolarization-activated channel predominantly expressed in thalamus, heart, and testis. *Proc Natl Acad Sci U S A*, *96*(16), 9391-9396.
- Shi, W., Wymore, R., Yu, H., Wu, J., Wymore, R. T., Pan, Z., . . . Cohen, I. S. (1999). Distribution and prevalence of hyperpolarization-activated cation channel (HCN) mRNA expression in cardiac tissues. *Circ Res*, *85*(1), e1-6.
- Shin, K. S., Rothberg, B. S., & Yellen, G. (2001). Blocker state dependence and trapping in hyperpolarization-activated cation channels: evidence for an intracellular activation gate. *J Gen Physiol*, *117*(2), 91-101.
- Stieber, J., Herrmann, S., Feil, S., Loster, J., Feil, R., Biel, M., . . . Ludwig, A. (2003). The hyperpolarization-activated channel HCN4 is required for the generation of



- pacemaker action potentials in the embryonic heart. *Proc Natl Acad Sci U S A*, *100*(25), 15235-15240. doi:10.1073/pnas.2434235100
- Stieber, J., Stockl, G., Herrmann, S., Hassfurth, B., & Hofmann, F. (2005). Functional expression of the human HCN3 channel. *J Biol Chem*, *280*(41), 34635-34643. doi:10.1074/jbc.M502508200
- Sunkara, M. R., Schwabe, T., Ehrlich, G., Kusch, J., & Benndorf, K. (2018). All four subunits of HCN2 channels contribute to the activation gating in an additive but intricate manner. *J Gen Physiol*, *150*(9), 1261-1271. doi:10.1085/jgp.201711935
- Thollon, C., Bedut, S., Villeneuve, N., Coge, F., Piffard, L., Guillaumin, J. P., . . . Vilaine, J. P. (2007). Use-dependent inhibition of hHCN4 by ivabradine and relationship with reduction in pacemaker activity. *Br J Pharmacol*, *150*(1), 37-46. doi:10.1038/sj.bjp.0706940
- Thon, S., Schmauder, R., & Benndorf, K. (2013). Elementary functional properties of single HCN2 channels. *Biophys J*, *105*(7), 1581-1589. doi:10.1016/j.bpj.2013.08.027
- Tibbs, G. R., Liu, D. T., Leybold, B. G., & Siegelbaum, S. A. (1998). A state-independent interaction between ligand and a conserved arginine residue in cyclic nucleotide-gated channels reveals a functional polarity of the cyclic nucleotide binding site. *J Biol Chem*, *273*(8), 4497-4505.
- Ulen, C., & Siegelbaum, S. A. (2003). Regulation of hyperpolarization-activated HCN channels by cAMP through a gating switch in binding domain symmetry. *Neuron*, *40*(5), 959-970.
- Varnum, M. D., & Zagotta, W. N. (1996). Subunit interactions in the activation of cyclic nucleotide-gated ion channels. *Biophys J*, *70*(6), 2667-2679. doi:10.1016/s0006-3495(96)79836-3
- Wainger, B. J., DeGennaro, M., Santoro, B., Siegelbaum, S. A., & Tibbs, G. R. (2001). Molecular mechanism of cAMP modulation of HCN pacemaker channels. *Nature*, *411*(6839), 805-810. doi:10.1038/35081088

- Wang, J., Chen, S., Nolan, M. F., & Siegelbaum, S. A. (2002). Activity-dependent regulation of HCN pacemaker channels by cyclic AMP: signaling through dynamic allosteric coupling. *Neuron*, 36(3), 451-461.
- Wang, J., Chen, S., & Siegelbaum, S. A. (2001). Regulation of hyperpolarization-activated HCN channel gating and cAMP modulation due to interactions of COOH terminus and core transmembrane regions. *J Gen Physiol*, 118(3), 237-250.
- Weber, I. T., Steitz, T. A., Bubis, J., & Taylor, S. S. (1987). Predicted structures of cAMP binding domains of type I and II regulatory subunits of cAMP-dependent protein kinase. *Biochemistry*, 26(2), 343-351.
- Williams, S. R., & Stuart, G. J. (2000). Site independence of EPSP time course is mediated by dendritic I(h) in neocortical pyramidal neurons. *J Neurophysiol*, 83(5), 3177-3182. doi:10.1152/jn.2000.83.5.3177
- Wongsamitkul, N., Nache, V., Eick, T., Hummert, S., Schulz, E., Schmauder, R., . . . Benndorf, K. (2016). Quantifying the cooperative subunit action in a multimeric membrane receptor. *Sci Rep*, 6, 20974. doi:10.1038/srep20974
- Xu, X., Vysotskaya, Z. V., Liu, Q., & Zhou, L. (2010). Structural basis for the cAMP-dependent gating in the human HCN4 channel. *J Biol Chem*, 285(47), 37082-37091. doi:10.1074/jbc.M110.152033
- Yellen, G. (2002). The voltage-gated potassium channels and their relatives. *Nature*, 419(6902), 35-42. doi:10.1038/nature00978
- Yu, F. H., Yarov-Yarovoy, V., Gutman, G. A., & Catterall, W. A. (2005). Overview of molecular relationships in the voltage-gated ion channel superfamily. *Pharmacol Rev*, 57(4), 387-395. doi:10.1124/pr.57.4.13
- Zagotta, W. N., Olivier, N. B., Black, K. D., Young, E. C., Olson, R., & Gouaux, E. (2003). Structural basis for modulation and agonist specificity of HCN pacemaker channels. *Nature*, 425(6954), 200-205. doi:10.1038/nature01922

Zhou, L., & Siegelbaum, S. A. (2007). Gating of HCN channels by cyclic nucleotides: residue contacts that underlie ligand binding, selectivity, and efficacy. *Structure*, *15*(6), 655-670. doi:10.1016/j.str.2007.04.012

## 8. Appendices

### Declaration

I hereby declare that:

1. I am aware of the current course of an examination for doctoral studies of the Faculty of Medicine at Friedrich Schiller University of Jena, Germany.
2. I have researched and written the presented thesis myself, no passages of text have been taken from third parties or own exam papers without having been identified. All tools, personal notifications, and sources used by me have been indicated in the thesis.
3. My doctoral supervisor Prof. Dr. Klaus Benndorf and advisor Dr. Jana Kusch have supported me in selecting and analyzing the material and in preparing the manuscript for publication. Most of the presented thesis has already published in a peer-reviewed scientific journal, Journal of General Physiology.
4. The assistance of any doctoral consultant has not been utilized and no third parties have either directly or indirectly received monetary benefits from the presented work or from related contents of the submitted thesis.
5. I have not submitted the thesis as an examination paper for state or other academic examinations.
6. I have not submitted the same, largely similar or any different treatises to another university as a dissertation.

Jena, 04.03.2019

-----

Mallikarjuna Rao Sunkara

[German translation]

## **Ehrenwörtliche Erklärung**

Ich erkläre hiermit, dass:

1. mir die geltende Promotionsordnung der Medizinischen Fakultät der Friedrich-Schiller-Universität Jena, Deutschland bekannt ist.
2. ich die vorliegende Arbeit selbst angefertigt habe, keine Textabschnitte von Dritten oder eigene Prüfungsarbeiten übernommen habe ohne diese zu kennzeichnen. Alle von mir verwendeten Hilfsmittel, persönlichen Mitteilungen und Quellen wurden in der Arbeit angegeben.
3. mein Betreuer Prof. Dr. Klaus Benndorf, und Dr. Jana Kusch haben mich bei der Auswahl und Analyse des Materials sowie bei der Erstellung des Manuskripts unterstützt hat. Der größte Teil der eingereichten Arbeit wurde bereits in einer von Experten begutachteten wissenschaftlichen Zeitschrift, Journal of General Physiology, veröffentlicht.
4. die Hilfe eines Promotionsberaters nicht in Anspruch genommen wurde und dass Dritte weder unmittelbar noch mittelbar geldwerte Leistungen von mir für Arbeiten erhalten haben, die im Zusammenhang mit dem Inhalt der vorgelegten Dissertation stehen.
5. ich die Dissertation noch nicht als Prüfungsarbeit für eine staatliche oder andere akademische Prüfung eingereicht habe.
6. ich die gleiche, eine in wesentlichen Teilen ähnliche oder eine andere Abhandlung bei einer anderen Hochschule als Dissertation nicht vorgelegt habe.

Jena, 04.03.2019

-----  
Mallikarjuna Rao Sunkara

## Acknowledgements

Firstly, I would like to express my sincere gratitude to esteemed supervisor Prof. Dr. Klaus Benndorf for his valuable and constructive suggestions during the planning and development of this research work. He offered me guidance, encouragements, and immense support throughout my Ph.D. and writing of this thesis. I would like to especially acknowledge his unconditional support in my tough times of both professionally and personally and made my path smoother. I am proud and privileged to have a doctoral supervisor like him.

Besides my supervisor, I would like to thank my special advisor Dr. Jana Kusch for her ever helping and ‘never saying no’ attitude. The vocabulary fails to express my heartfelt gratitude and immeasurable indebtedness for her backing in my ups and downs throughout my thesis. She has been the source of excellent supervision, advice, motivation, guidance, and caring during my Ph.D. journey, and also especially in the most difficult time when I had to hurry to finish my thesis in which I need to move on. Without her generous guidance and persistent assistance, this dissertation would have not been successful.

Also, I sincerely thank all of my beloved colleagues who helped and suggested me several techniques and scientific knowledge both. I appreciate the contributions of my fellow Ph.D. students whose time, ideas, comments, criticism, support, and encouragement led to the success of my doctoral project. Moreover, I want to express my sincere gratitude to my thesis committee members who carefully corrected my thesis and offered me brilliant suggestions for the oral defense.

Lastly, I praise the enormous amount of energy and love from God and my family; mother, father, and younger brother from India. I sincerely express my warmest gratitude to the most important person in my life, my wife, who has shown great patience and understanding during the odd time of my life.

- Mallikarjuna Rao Sunkara